

Scaled Particle Theory and the Length-scales Involved in Hydrophobic Hydration of Aqueous Biomolecular Assemblies

Henry S. Ashbaugh and Lawrence R. Pratt

*Theoretical Division, Los Alamos National Laboratory, Los Alamos, NM 87545,
USA*

(Dated: May 1, 2019)

Abstract

Hydrophobic hydration plays a crucial role in self-assembly processes over multiple-length scales, from the microscopic origins of inert gas solubility in water, to the mesoscopic organization of proteins and surfactant structures, to macroscopic phase separation. Many theoretical studies focus on the molecularly detailed interactions between oil and water, but the extrapolation of molecular-scale models to larger length scale hydration phenomena is sometimes not warranted. Scaled particle theory approaches are based upon an interpolative view of that microscopic→macroscopic issue. We revisit the scaled particle theory proposed thirty years ago by Stillinger (*J. Soln. Chem.* **2**, 141-158 (1973)), adopt a practical generalization, and consider the implications for hydrophobic hydration in light of our current understanding. The generalization is based upon identifying a molecular length, implicit in previous applications of scaled particle models, that provides an effective boundary radius for joining microscopic and macroscopic descriptions. We demonstrate that the generalized theory correctly reproduces many of the anomalous thermodynamic properties of hydrophobic hydration for molecularly sized solutes, including solubility minima and entropy convergence, successfully interpolates between the microscopic and macroscopic extremes, and provides new insights into the underlying molecular mechanisms. The model considered here serves as a reference for theories that bridge microscopic and macroscopic hydrophobic effects. The results are discussed in terms of length scales associated with component phenomena; in particular we first discuss the length locating a micro-macroscopic boundary identified by the theory, then we discuss in turn the Tolman length that leads to an analogous length describing curvature corrections of a surface area model of hydrophobic hydration free energies, and the length scales on which *entropy convergence* of hydration free energies are expected.

Contents

I. Introduction	3
II. A Primer on Scaled Particle Theory	9
A. Classic Scaled Particle Theory	9
B. Revised Scaled Particle Theory	12
C. Computational Implementation	14
III. Application to Hydrophobic Hydration	14
A. Cavity contact correlation functions: the micro-macro boundary	14
B. Hydration thermodynamics of hydrophobic species: temperature signatures and solubility minima	17
C. Surface area dependence of hydration thermodynamic properties: the Tolman length and curvature corrections	19
D. Entropy convergence and solute size	21
IV. Summary and Conclusions	25
Acknowledgements	27
References	27
Figures	31

I. INTRODUCTION

The adage ‘oil and water don’t mix’ dominates thinking about hydrophobic effects that are upheld, nearly universally, as the primary thermodynamic impetus for a number of important aqueous solution phenomena, including the environmental fate of pollutants, surfactant assembly, biological membrane formation, and the folding of globular proteins (Blokzijl and Engberts, 1993; Kauzmann, 1959; Simonson, 2003; Tanford, 1980). Enigmatic temperature signatures — such as the fact that many soluble proteins unfold both upon heating *and* cooling — offer the primary puzzles of hydrophobic effects, and are characteristic of the aqueous milieu. An organized ability to reproduce these temperature signatures

from basic principles is essential for understanding the temperature range of functional behavior of biophysical structures, and of aqueous phase nanotechnology invented by analogy with the molecular machinery of biophysics. An important aspect of these puzzles is that the hydrophobic temperature signatures are strongly affected by the spatial or length scale of the hydrophobic solution structures. This review focuses on recent progress in unraveling the puzzles of temperature signatures and length scales characteristic of hydrophobic hydration.

The aqueous phase solutes that motivate study of hydrophobic effects are typically molecularly complicated, often water soluble but amphiphilic chain molecules. Thus, hydrophobic phenomena usually do not occur in isolation. Researchers studying these systems have been comfortable, however, with a hydrophilic-hydrophobic dichotomy. A helpful review of electrostatic hydrophilic interactions involved in protein molecular structure with an emphasis on the different lengths scales involved appeared recently (Simonson, 2003). That review can serve to supply a current picture of aqueous phase interactions complementary to the hydrophobic effects discussed here. It is not uncommon for aqueous solutions interactions that have been clearly identified, such as classic electrostatic interactions, to provide by this hydrophilic-hydrophobic dichotomy an identification of hydrophobic effects (Pratt, 1998). This is particularly true if the temperature dependences of the complementary interactions are also somewhat murky! Our review here will emphasize standard model solutes, inert excluded volume models, that do permit study of hydrophobic effects exclusively. Gases that are sparingly soluble in water, and small hydrocarbon molecules, can be brought simply into correspondence with hardcore molecular models. These simple systems and models permit precision in isolating the peculiar temperature signatures that are the target of studies of hydrophobic effects.

Experimental heats of hydration, determined from high precision calorimetric studies, show that unfavorable entropies of transferring nonpolar solutes into water dominate hydration free energies at room temperature, and are only partly compensated by favorable dissolution enthalpies. These measurements are incongruous with *regular solution* notions, which ascribe insolubility to unfavorable cohesive interactions between the solute and water compared to water with itself (Lazaridis, 2001). Of foremost importance, the entropies and enthalpies of hydrophobic hydration are strongly temperature dependent, following from the large positive transfer heat capacities observed. Thus, at elevated temperatures the roles of

entropy and enthalpy are reversed, with unfavorable enthalpies dominating hydration free energies, partly compensated by favorable entropies. The resulting solubilities of nonpolar gases are nonmonotonic, exhibiting a solubility minimum between 310 K and 350 K. Analogously, proteins undergo hot *and* cold denaturation (Brandts, 1964; Franks and Hatley, 1991) as noted above, while ionic and nonionic surfactants display a minimum in their critical micelle concentrations with respect to temperature (Chen *et al.*, 1998a,b), pointing to a common underlying mechanism with the solubility behavior of nonpolar species. Careful analysis of the experimental entropy changes upon hydrocarbon hydration, as a function of temperature, reveals that these curves intersect at an entropy change close to zero at ≈ 385 K (Baldwin, 1986; Lee, 1991; Makhatadze and Privalov, 1995; Muller, 1993; Murphy *et al.*, 1990; Privalov, 1979; Privalov and Gill, 1988). The coincidence of this entropy convergence temperature for hydrocarbons with comparable behavior in protein unfolding has been used as empirical justification for the hydrophobic core model for protein folding, and has influenced the interpretation of biomolecular assembly. But in the complex context of soluble protein molecules, a clear relevance of entropy convergence can be questioned (Robertson and Murphy, 1997).

Puzzlements about hydrophobic effects derive from entropic origins in molecular-scale hydration structure. The theoretical description of hydrophobic effects has recently progressed markedly, and the understanding of the roles played by this entropic force in the functional stabilization of micelles, membranes, soluble proteins, and hierarchical biomolecular aggregation in aqueous solution has similarly advanced. It is now understood that the scaled particle theories can properly describe primitive hydrophobic effects associated with the hydration of simple mono-atomic species. Scaled particle theories identify — inadvertently at first, but firmly nonetheless — a length that separates a microscopic from a macroscopic description of hydration structure. This point has not been widely appreciated. This radial length establishes a boundary at which microscopic and macroscopic descriptions of hydration structure join effectively. A basic understanding of this micro-macroscopic boundary region, together with primitive constitutive information specific to liquid water, can provide an effective description of hydrophobic effects for meso-scale aqueous assembly processes.

Much of the recent progress in understanding hydrophobic effects can be discussed on the basis of length scales associated with component phenomena of long standing interest. This paper lays out that basic view which generalizes the application of scaled particle theories,

establishes on that basis the micro-macroscopic boundary length, and then discusses in turn the Tolman length that leads to an analogous length describing curvature corrections of a surface area model of hydrophobic hydration free energies, and the length scales on which *entropy convergence* of hydration free energies can be expected.

It has been traditionally argued that hydrophobic effects for molecular solutes stem from orientational constraints in the hydration shell of nonpolar solutes to maintain the integrity of a hydrogen-bonding water network forming cage-like structures or microscopic *icebergs* (Frank and Evans, 1945). While providing a language for discussing hydrophobic hydration suggestive of the molecular origins of the insolubility of oils, this interpretation has done nothing to resolve the relative magnitudes of the opposing enthalpic and entropic contributions to hydration. Theoretical studies of the impact of local clatharate formation about krypton in liquid water have demonstrated that such ordered structures are far too unfavorable to play a role in hydration thermodynamics (Ashbaugh *et al.*, 2003). Experimental probes of the local structure of water proximal to purely nonpolar solutes are scarce, and hampered by the low solute concentrations attainable. The structures that have been measured by neutron and X-ray scattering techniques suggest that while water surely adopts orientational preferences in the hydration shell of nonpolar moieties, the solute induced structure is more disordered than that in ice or clatharate hydrates (Bowron *et al.*, 1998a,b; Broadbent and Neilson, 1994; DeJong *et al.*, 1997; Filippioni *et al.*, 1997).

Molecular level investigations of hydrophobic hydration have been largely theoretical and simulation efforts (Henderson, 2002; Hummer *et al.*, 1998, 1996; Pierotti, 1976; Pohorille and Pratt, 1990; Pratt, 2002; Pratt and Pohorille, 1992; Stillinger, 1973). Water structure and orientational preferences in the vicinity of hydrophobic species has been connected to the characteristic entropies of hydrophobic hydration through the application of a statistical mechanical correlation function expansion for the entropy (Ashbaugh and Paulaitis, 1996; Lazaridis and Paulaitis, 1992; Silverstein *et al.*, 2001). More recently, information theory (IT) (Hummer *et al.*, 1998, 2000) with tentacles to the Pratt-Chandler (Pratt and Chandler, 1977) and the Gaussian field (Chandler, 1993; Lum *et al.*, 1999) theories, has provided a quantitative link between the microscopic density fluctuations determined from water oxygen pair correlations and the hydration free energies of hard solutes. More importantly, IT implicates the unique equation-of-state properties of water as a dominant factor in hydrophobic hydration, differentiating water from other com-

mon solvents. In addition to capturing temperature and pressure effects associated with hydrophobic hydration and interactions, (Hummer *et al.*, 1998) IT provides a facile explanation of the enhanced solubility of nonpolar species in D_2O compared to H_2O as a result of differences in the isothermal compressibilities of these isotopic alternative forms of water (Hummer *et al.*, 2000).

The distinction between molecular hydrophobic effects, quantified by hydrocarbon-water transfer free energies, and the hydrophobic forces that drive assembly on larger length scales was first noted by Tanford (Tanford, 1979). His observation was based on the large discrepancy between the measured water-hydrocarbon interfacial tension and the effective microscopic surface tensions obtained from hydrocarbon solubility data. Moreover, the relationship between macroscopic and microscopic surface tensions is contentious due to fundamental differences in their temperature dependencies. More recent examples of the distinction between molecular and macroscopic hydrophobic interactions is found in measurements of the long-range attractive force between macroscopic hydrophobic surfaces (Christenson and Claesson, 1988; Israelachvili and Pashley, 1982; Pashley *et al.*, 1985) which have not been explained on the basis of molecular hydrophobic effects. Vibrational sum frequency experiments suggest that aqueous hydrogen-bonding is weaker at macroscopic water-carbon tetrachloride and water-hexane interfaces than that near individual hydrophobic species dissolved in water (Scatena *et al.*, 2001). The lack of a definitive interpretation of these surface force measurements, and the changes in water energetics at macroscopic interfaces underscores the need for a quantitative theory of hydrophobic phenomena beyond molecular hydrophobic effects. In general, the need for a unified, quantitative description of both molecular and macroscopic hydrophobic phenomena arises because hydrophobic driving forces play an important role in self-assembly on multiple length scales and the fact that quantitative descriptions of these driving forces are derived from molecular solubility data, macroscopic interfacial tension measurements, or interpolations of these quantities (Ashbaugh *et al.*, 1999; Ashbaugh and Paulaitis, 2001; Hermann, 1977; Sharp *et al.*, 1991; Tanford, 1979).

Chandler and coworkers (Lum *et al.*, 1999) have suggested bridging these vast length scales by integrating a Gaussian field theory for molecular level fluctuations with mean-field theory for larger scale fluctuations ultimately responsible for macroscopic phase transitions. Their approach successfully predicts many of the thermodynamic anomalies characteristic of

small molecule hydration, and goes further, predicting the onset of long-range hydrophobic forces between surfaces as a result of a aqueous liquid-vapor phase transition in confined geometries. Indeed surface force apparatus studies of the long-range hydrophobic interaction observed cavitation between nonpolar surfaces (Christenson and Claesson, 1988), consistent with theoretical predictions. Mean-field modeling and simulations of methane clusters, however, suggest that when ubiquitous attractive dispersion interactions between water and hydrophobic surfaces are taken into account, the length scales over which confinement induces an aqueous phase transition is suppressed (Ashbaugh and Paulaitis, 2001; Truskett *et al.*, 2001). Moreover, experiments on the effects of electrolyte addition and degassing on the range of surface forces, and the stability of surfactant free aqueous emulsions challenge the theoretical predictions (Considine *et al.*, 1999; Kokkoli and Zukoski, 1998; Pashley, 2003).

A conceptual basis for unifying molecular and macroscopic hydrophobic hydration can be found in scaled particle theory (SPT). Thirty years ago Frank Stillinger (Stillinger, 1973) presented an influential paper on the application of the classic SPT of Reiss (Pierotti, 1976; Reiss, 1965, 1977; Reiss *et al.*, 1959) to the hydration thermodynamics of purely excluded volume solutes. The purpose of that paper was, in part, to illuminate the pitfalls and difficulties in applying classic SPT, originally developed for hard-sphere fluids, to aqueous solvents. In doing so Stillinger opened up new avenues of inquiry into hydrophobic hydration within the context of SPT. Nevertheless, direct exploration of the validity and consequences of Stillinger's suggested revised theory have been rare (Pratt and Pohorille, 1992, 1993). We presently revisit SPT and critically discuss its implications in light of our current understanding of hydrophobic hydration. For the first time, we demonstrate that the revised SPT reproduces many of the characteristic thermodynamic signatures of molecular hydrophobic effects and can be used to extend the results of molecular simulations of small hydrophobic hard solutes in water to meso- and macroscopic surface hydration. The present analysis provides insights into the differences and similarities for hydrating molecular and macroscopic surfaces. In addition, we examine the validity of surface area correlations commonly used in biophysical models for hydration thermodynamics over a range of length scales, as well as the origins of entropy convergence behavior at molecular lengths scales and how solute size moderates the convergence temperature.

II. A PRIMER ON SCALED PARTICLE THEORY

A. Classic Scaled Particle Theory

The chemical potential of a hydrated mono-atomic solute, S , can be expressed formally as

$$\mu_S(aq) = kT \ln [\rho_S(aq)\Lambda_S^3] + \mu_S^{ex}(aq) \quad (1)$$

where we have adopted Ben-Naim's standard state in the definition of the chemical potential (Ben-Naim and Marcus, 1984). Here k is Boltzmann's constant, T is the temperature, $\rho_S(aq)$ is the solute number density in the solution, Λ_S is the thermal de Broglie wavelength of the solute, and μ_S^{ex} is the excess chemical potential, *i.e.*, the coupling work of turning on interactions between the solute and water, which disappears if those interactions vanish. At thermal equilibrium the Ostwald partition coefficient determining the distribution of the solute between an aqueous and ideal gas ($\mu_S^{ex}(ideal) = 0$) phase at infinite dilution is (Pollack, 1991)

$$K_{eq} = \frac{\rho_S(aq)}{\rho_S(ideal)} = \exp [-\mu_S^{ex}(aq)/kT]. \quad (2)$$

Thus, the excess chemical potential is central to resolving the aqueous solubility of the solute. Confining our discussion to impenetrable hard sphere (HS) solutes, the solute excess chemical potential in water is

$$\mu_S^{ex}(aq) = -kT \ln p_0(R) \quad (3)$$

where the insertion probability, $p_0(R)$, is the probability that a solute sized stencil randomly placed in water is devoid of water oxygen centers; this follows directly from Widom's potential distribution theorem for species interacting with a hard potential (Pratt *et al.*, 1999; Widom, 1982). The solvent accessible radius, R , is the radius of closest approach between the solute center and a water oxygen. The solvent accessible radius is the sum of the effective hard sphere radius of water and the hard van der Waals radius of the solute, *i.e.*, $R = (\sigma_{WW} + \sigma_{SS})/2$. As $R \rightarrow 0$, the solute van der Waals radius becomes negative, and the solute can penetrate the nominal excluding volume of water molecules. While physically novel, the negative van der Waals radius stems from the requirement that R must equal zero for the solute to be completely absent from solution. This requirement poses no conceptual

or mathematical difficulties on the underlying statistical thermodynamic formulation. In this context, the insertion probability can be viewed as the fractional free (or *available*) volume in solution available for the solute to occupy, *i.e.*, $p_0(R) = V_{free}/V_{total}$.

A physical picture of $p_0(R)$ is illustrated in Figure 1. Given a molecular snapshot of liquid water (left hand box in Fig. 1), taken for example from a computer simulation, V_{free} for a given cavity radius is determined by the points at which a cavity can be successfully inserted yielding a negative image templated by the aqueous configuration (right hand box in Fig. 1). As would be expected V_{free} decreases with increasing cavity radius, and as such successful insertions become increasingly rare. $p_0(R)$ is subsequently determined as an ensemble average over a large number of molecular configurations.

An alternative relationship for the chemical potential that draws a connection to the structure of water in the vicinity of the solute is

$$\frac{\mu_S^{ex}(aq)}{kT} = \int_0^R \rho_W G(r) 4\pi r^2 dr \quad (4)$$

where $\rho_W G(r)$ is the density of water in contact with a hard solute cavity of radius r . The product $\rho_W kT G(r)$ has units of force per unit area and can be thought of as a pressure due to solvent collisions with the hard solute surface. The chemical potential then is the reversible pressure-volume work required to grow the solute into solution. The etymology of scaled particle theory is derived from this expression (Reiss, 1965, 1977) since the solute is introduced by scaling it up from a particle with a solvent accessible radius of zero to a final size of R . The relationship between the contact function and the insertion probability is

$$G(R) = -\frac{1}{4\pi R^2 \rho_W} \frac{\partial \ln p_0(R)}{\partial R} , \quad (5)$$

as determined by differentiation of Eq. 4. For sufficiently small solute cavities that only one solvent molecule might fit within the cavity boundary, the insertion probability is

$$p_0(R \rightarrow 0) = 1 - \frac{4\pi}{3} \rho_W R^3 . \quad (6)$$

The corresponding expression for the contact correlation function is

$$G(R \rightarrow 0) = \frac{1}{1 - \frac{4\pi}{3} \rho_W R^3} . \quad (7)$$

These expressions are exact in hard sphere fluids and accurate in solvents with realistic interactions for cavities up to a radius of $R \approx \sigma_{WW}/2$, where the solute corresponds to a

point particle with a van der Waals radius of zero. Packing considerations indicate that between solvent accessible radii of $\sigma_{WW}/2$ and $\sigma_{WW}/\sqrt{3}$ at most two solvent centers might fit within the solute cavity. Increasingly more solvent molecules can fit within cavities of increasing size, requiring information on dauntingly more complex multi-body correlations.

In the limit of a macroscopically large cavity, the contact correlation function can be represented as an asymptotic expansion in $1/R$

$$G(R) \sim \sum_{j \geq 0} \frac{G_j}{R^j}. \quad (8)$$

Retaining contributions up to $j = 2$ yields an expression equivalent in form to that required by classical thermodynamics for the force acting on the cavity surface (Henderson, 2002; Pierotti, 1976; Reiss, 1965, 1977; Stillinger, 1973)

$$kT\rho_W G(R) \sim p + \frac{2\gamma_\infty}{R} - \frac{4\gamma_\infty\delta}{R^2} \quad (9)$$

where p is the bulk pressure (typically assumed to be equal to the liquid saturation pressure p_{sat}), γ_∞ is the surface tension of a flat interface, and δ , the Tolman length (Tolman, 1949), describes the initial curvature correction to the surface tension. The third order coefficient, G_3 is necessarily equal to zero so that the chemical potential is free of logarithmic contributions, as required by the general theory (Stillinger and Cotter, 1971). The relationship between higher order terms of the contact correlation function and classical thermodynamic quantities is uncertain. Such considerations motivated (Reiss *et al.*, 1959) to truncate Eq. 8 after the first curvature correction in order to develop a tractable, physically reasonable model for the contact correlation function.

Evaluating the $j=0$ term in Eq. 8 by comparison with the classical thermodynamic expression and the first and second order terms in the expansion by requiring the microscopic and macroscopic limits smoothly meet at $\sigma_{WW}/2$, the expression

$$G(R) = \begin{cases} \frac{1}{1 - \frac{4\pi}{3} \rho_W R^3}, & R \leq \sigma_{WW}/2 \\ \frac{p_{sat}}{kT\rho_W} + \left[\frac{2-\eta}{(1-\eta)^2} - \frac{2p_{sat}}{kT\rho_W} \right] \left(\frac{\sigma_{WW}}{2R} \right) \\ + \left[-\frac{(1+2\eta)}{(1-\eta)^2} + \frac{p_{sat}}{kT \rho_W} \right] \left(\frac{\sigma_{WW}}{2R} \right)^2, & R > \sigma_{WW}/2 \end{cases} \quad (10)$$

is obtained for the contact correlation function. Here $\eta = \frac{\pi}{6} \rho_W \sigma_{WW}^3$ is the solvent packing

fraction. Integration of the contact correlation function yields the excess chemical potential

$$\frac{\mu_S^{ex}}{kT} = \begin{cases} \ln \left(1 - \frac{4\pi}{3} \rho_W R^3 \right) , & R \leq \sigma_{WW}/2 \\ \left[-\ln(1-\eta) + \frac{9\eta^2}{2(1-\eta)^2} - \frac{\eta p_{sat}}{kT\rho_W} \right] + \left[-\frac{3\eta(1+2\eta)}{(1-\eta)^2} + \frac{3\eta p_{sat}}{kT\rho_W} \right] \left(\frac{2R}{\sigma_{WW}} \right) \\ \quad + \left[\frac{3\eta(2+\eta)}{2(1-\eta)^2} - \frac{3\eta p_{sat}}{kT\rho_W} \right] \left(\frac{2R}{\sigma_{WW}} \right)^2 + \frac{\eta p_{sat}}{kT\rho_W} \left(\frac{2R}{\sigma_{WW}} \right)^3 , & R > \sigma_{WW}/2 . \end{cases} \quad (11)$$

Eqs. 10 and 11 constitute the classic SPT originally developed for HS solvents (Reiss, 1965, 1977), which has subsequently been applied to water by Pierotti (Pierotti, 1976) and Lee and coworkers (Lee, 1985). Fundamental difficulties arise in the application of classic SPT to water, however, including the erroneous prediction that the surface tension of water increases with temperature and passes through a maximum near 425K (Stillinger, 1973).

B. Revised Scaled Particle Theory

The scaled particle model described above incorporates little molecular detail, other than the effective HS diameter, that might differentiate water from other solvents, and thereby limits the interpretation of complex hydration phenomena. The insertion probability is formally expressed on the basis of solvent structure by an inclusion-exclusion development (Reiss, 1965, 1977; Stillinger, 1973)

$$p_0(R) = 1 + \sum_{n \geq 1} \frac{(-\rho_W)^n}{n!} \int_{V(R)} \dots \int_{V(R)} g^{(n)}(\mathbf{r}_1 \dots \mathbf{r}_n) d^3r_1 \dots d^3r_n \quad (12)$$

where $V(R) = 4\pi R^3/3$ is the observation volume, and $g^{(n)}(\mathbf{r}_1 \dots \mathbf{r}_n)$ are the n -body solvent oxygen distribution functions. The terms in this series vanish for n exceeding the maximum number of solvent molecular centers that can be packed into a sphere of volume $4\pi R^3/3$. It is on this basis that the limiting results Eq. 6 are established. As noted above, these distribution functions are complicated and impractical to evaluate beyond the pair-distribution function ($n = 2$). Considering the small cavity pair-correlation contribution and the asymptotic macroscopic thermodynamic limits, Stillinger proposed a revised expression for the cavity correlation function (Stillinger, 1973)

$$G(R) = \begin{cases} \frac{1 + \frac{\pi \rho_W}{R} \int_0^{2R} g^{(2)}(r) r^2 (r-2R) dr}{1 - \frac{4\pi}{3} \rho_W R^3 + \left(\frac{\pi \rho_W}{R} \right)^2 \int_0^{2R} g^{(2)}(r) (r^3/6 - 2R^2 r + 8R^3/3) dr} , & R \leq R^* \\ \frac{p}{kT\rho_W} + \frac{2\gamma_\infty}{kT\rho_W R} - \frac{4\gamma_\infty \delta}{kT\rho_W R^2} + \frac{\lambda}{R^4} , & R > R^* \end{cases} \quad (13)$$

where R^* is the point at which three-body correlations begin to contribute to the cavity insertion probability. While the experimental pressure, surface tension, density, and solvent

radial distribution function are employed, δ and λ are treated as adjustable parameters chosen so that the small cavity and macroscopic limits of the contact correlation function join smoothly at R^* . This expression incorporates molecular information on the pair structure of water as well as the known macroscopic properties of bulk water and its interfacial behavior, and thereby is expected to discriminate more sensitively between water (Ashbaugh and Paulaitis, 2001) and other solvents (Huang and Chandler, 2000). Indeed, it has been demonstrated by extensive molecular simulations that Eq. 13 provides a description superior to the classic SPT expression Eq. 10 of the solvent contact density for solutes several times larger than the solvent.

Stillinger's revised SPT prediction for $G(R)$ relies on the assumption that multi-body water correlations at intermediate, but molecularly sized, solute radii are adequately represented by the parameters δ and λ fitted at a single point R^* . Consideration of alternative values for R^* shows that this parameter is associated with the greatest sensitivity displayed by this revised scaled particle theory (Pratt and Pohorille, 1992). That procedure might be improved by obtaining these parameters over a range of radii which include solute sizes for which multi-body correlations are significant. While this information is not readily available experimentally, multi-body correlation contributions to the HS solute chemical potential can be interrogated by direct evaluation of the insertion probabilities from molecular simulations of water. In the spirit of Stillinger's revised SPT, we interpolate between the chemical potential evaluated from explicit simulation and the macroscopic thermodynamic limit

$$\mu_S^{ex}(R) = -kT \ln p_0(R)|_{sim} f(R) + \mu_S^{ex}(R)|_{macro} [1 - f(R)] \quad (14)$$

where $f(R)$ is a switching function equal to one below R_{sim} and zero above R_{macro} that smoothly interpolates between these between these two limits. Presently we use a cubic spline interpolating function, though other reasonable functions yield essentially indistinguishable predictions. The macroscopic chemical potential, determined by integration of the macroscopic cavity expression Eq. 13 in

$$\mu_S^{ex}(R)|_{macro} = -\frac{4\pi kT \rho_W \lambda}{R} + \epsilon - 16\pi R \gamma_\infty \delta + 4\pi R^2 \gamma_\infty + \frac{4\pi}{3} R^3 p_{sat} \quad (15)$$

Rather than fitting the microscopic and macroscopic limits at a single point as in Eq. 13, the parameters δ , λ , and the integration constant ϵ are fitted to the simulation results between R_{sim} and R_{macro} . The contact correlation function is then determined by differentiation

of the chemical potential (Eq. 5). An additional benefit of fitting Eq. 15 to the simulation insertion probabilities is that we do not have to evaluate numerically first and second derivatives of the simulated insertion probabilities, which become more statistically uncertain with increasing cavity size.

C. Computational Implementation

Water configurations were generated using Monte Carlo simulations in the canonical ensemble (Frenkel and Smit, 2002). Bulk water was modeled using 268 SPC/E water molecules with periodic boundary conditions (Berendsen *et al.*, 1987). SPC/E was chosen because, for a simple three point potential, it provides one of the more accurate representations of the structure, equation-of-state, and interfacial tension of liquid water over a broad range of temperatures (Alejandre *et al.*, 1995; Hura *et al.*, 2003). Lennard-Jones potential interactions were evaluated smoothly truncating the potential based on the separation of water oxygens between 9.5Å and 10Å, while longer ranged electrostatic interactions were calculated using Ewald summation with conducting boundary conditions (Frenkel and Smit, 2002). Simulations were carried out from 260 K to 470 K in 10 K increments at the experimental liquid density along the saturation curve. After an equilibration phase of at least 10^5 MC passes (where one pass corresponds to one attempted move per water molecule with 30% move acceptance), 5×10^6 MC production passes were carried out for analysis of thermodynamic averages. After every 50 MC passes, 10^5 particle insertions were attempted to determine $p_0(R)$ for a total of 10^{10} insertions at each temperature. Statistical uncertainties were determined by grouping results into block averages over 10^6 MC passes each.

III. APPLICATION TO HYDROPHOBIC HYDRATION

A. Cavity contact correlation functions: the micro-macro boundary

The cavity contact function at 300K is shown in Fig. 2. Beginning at a value of one at zero radius, the cavity contact density increases with increasing HS cavity size. Simulation values of $G(R)$ appear to plateau at a maximum at approximately 3Å. Just beyond this radius, the simulation results for $G(R)$ become progressively noisy as a result of poor sampling of infrequent large cavity fluctuations. A dominating observation is that this curve imposes a

non-arbitrary definition of a length scale for the present problem: the radius R_{max} , at which $G(R)$ is a maximum. Solutes with smaller radii are identified as intrinsically molecular scale. The description of the hydration of solutes of larger radii can be built from a macroscopic perspective. An interpolative strategy extending to large solutes, such as that adopted here, is likely to be particularly effective if the region at which the molecular and macroscopic expressions are joined encompasses R_{max} . The revised SPT fit, determined by differentiation of Eq. 14 fitted to the simulation insertion results between $R_{sim} = 2.5\text{\AA}$ and $R_{macro} = 3.5\text{\AA}$, accurately extends $G(R)$ to HS cavities considerably larger than observable with any statistical accuracy during the molecular simulations. The revised SPT result places the maximum contact density at $R = 3.0\text{\AA}$ where $G(R)$ achieves the value of ≈ 2.3 . Solutes of this size are candidates for ‘most hydrophobic’ because the compressive force exerted by the solvent is largest in this case; see Fig. 3. Beyond this maximum, water pulls away from the cavity surface with increasing size, at length scales of $\approx 10\text{\AA}$ the contact density equals the bulk density of water, decreasing further for larger cavities. In the limit $R \rightarrow \infty$, the contact correlation approaches $\frac{p_{sat}}{\rho_W kT} \approx 2 \times 10^{-5}$ for water at 300K, and does not impact the contact correlation function for molecular and mesoscopic cavities at any of the temperatures considered.

This apparently anomalous dewetting behavior was anticipated by (Stillinger, 1973), and has only recently been confirmed by molecular simulations in Lennard-Jones and aqueous solvents (Ashbaugh and Paulaitis, 2001; Huang and Chandler, 2000). The surface dewetting has been previously interpreted in terms of an effective expulsion potential between water and the solute cavity (Hummer and Garde, 1998; Weeks *et al.*, 1998). In bulk water, the individual water molecules feel attractive interactions with the other water molecules, and the average force on a water molecule in the bulk is zero. To approach a large solute, however, a water molecule must shed hydration partners, or limit their possible configurations. This unbalances the interactions with the aqueous medium and gives rise to an additional repulsive force between a water molecule and the surface. If the solute is unable to compensate for these lost interactions and counter the cavity expulsion potential, water will be repelled by the surface.

The classic SPT prediction for the contact correlation function (Eq. 10) is in qualitative agreement with the simulation and revised SPT results (Fig. 2). Classic SPT predicts a maximum in the contact density, followed by a decrease to values below the bulk density of

water with increasing cavity radius. The quantitative agreement is poor, however, even if the effective HS diameter of water is treated as an adjustable parameter. Notably, classic SPT predicts that the maximum in $G(R)$ is shifted to smaller radii of $\approx 2\text{\AA}$. This shift likely results from differences in the packing in HS fluids versus hydrogen-bonded water networks. Water has a more open structure favoring larger cavities than the less structured HS fluid at comparable packing fractions (Pohorille and Pratt, 1990; Pratt and Pohorille, 1992). The resulting maximum in the pressure acting on the solute surface, $kT\rho_W G(R)$, then is shifted out to larger cavity radii for water.

If the objective of classic SPT is to reproduce the chemical potentials of solutes using Eq. 11 up to solvent accessible radii of $\approx 3.3\text{\AA}$, encompassing the sizes of a number of nonpolar gases, a typical HS diameter of water fitted to experimental data is 2.7\AA (Lee, 1985), though a more appropriate value based on the simulation results reported in Fig. 2 is 2.8\AA . In this case, the fitted radius of water splits the difference between the classic SPT over-prediction of $G(R)$ at intermediate radii and the under-prediction at radii close to the maximum solute size to balance out these inaccuracies in the calculation of the chemical potential. This HS size for water then is a consequence of the fitting, and does not contribute to the interpretation of the molecular signatures of hydrophobicity. Indeed, if we extend the predictions of classic SPT outside the range fitted for small solutes, we find the theory under-predicts the hydration free energies of mesoscopic cavities and that a larger water diameter ($\sigma_{WW} \approx 2.9\text{\AA}$) is required to match the dewetting observed in $G(R)$ (Fig. 2). This cavity size dependent HS diameter for water, much less its temperature dependence, results from the fact that σ_{WW} is the only molecular parameter in classic SPT for the interpretation of hydration effects. While this solute size dependence may seem small, the chemical potential depends on the integral of the cavity contact correlation function and small differences in the solvent diameter significantly alter the predictions. Broadly viewed, this is the natural observation that slight adjustment of boundary information in boundary value problems can make large changes in the solution away from the boundary.

Revised SPT predictions for $G(R)$ as a function of temperature are shown in Fig. 4. While all the curves are qualitative similar, the magnitude of the contact correlation function decreases with increasing temperature. Classic SPT fails to describe the temperature dependence of $G(R)$ and inferences similar to those described above regarding the applicability of classic SPT to the contact correlation function in water apply. In the following sections

we use these revised SPT results to draw conclusions regarding the size and temperature dependence of the hydration of hydrophobic hard spheres.

B. Hydration thermodynamics of hydrophobic species: temperature signatures and solubility minima

The hydration free energy of a methane sized ($R = 3.3\text{\AA}$) HS in water as a function of temperature along the saturation curve is shown in Fig. 5. The simulation results for the chemical potential pass through a maximum at $\approx 400\text{K}$, at which point the hydration entropy defined by $s_S^{ex} = -\partial\mu_S^{ext}/\partial T|_{sat}$ is zero. To extract the enthalpy and entropy of hydrophobic hydration from the chemical potential, we assume that the heat capacity $\partial h_S^{ex}/\partial T|_{sat} = -\partial s_S^{ex}/\partial T|_{sat} = c_0^{ex}$ is independent of temperature. In this case, the hydration enthalpy, entropy, and free energy are

$$h_S^{ex} = h_0^{ex} + (T - T_0) c_0^{ex}, \quad (16\text{-a})$$

$$s_S^{ex} = s_0^{ex} + \ln\left(\frac{T}{T_0}\right) c_0^{ex}, \quad (16\text{-b})$$

$$\mu_S^{ex} = \mu_0^{ex} + (T - T_0) (c_0^{ex} - s_0^{ex}) - T \ln\left(\frac{T}{T_0}\right) c_0^{ex}, \quad (16\text{-c})$$

respectively, where the subscript 0 corresponds to the value of the individual thermodynamic properties at the reference temperature T_0 .

The enthalpy and entropy of hydration of the methane-sized HS solute is shown alongside the fitted free energy in Fig. 5. As expected for hydrophobic hydration, the hydration entropy is negative and unfavorable at room temperature (Blokzijl and Engberts, 1993; Kauzmann, 1959; Tanford, 1980). With increasing temperature the entropy changes sign indicative of a positive heat capacity increment. The entropy and heat capacity at 298K for the HS solute are -69.5 J/(mol K) and 214 J/(mol K), respectively, which is in excellent agreement with the experimental values for the entropy and heat capacity of -66.7 J/(mol K) and 209 to 237 J/(mol K) for methane at 298K. Over most of the temperature range considered, the HS hydration enthalpy is positive and unfavorable for hydration, in disagreement with the experimental enthalpy for methane of -11.5 kJ/mol at 298K (Lazaridis and Paulaitis, 1992), largely a result of the neglect of attractive interactions with water. The *iceberg* hypothesis of Frank and Evans (Frank and Evans, 1945) suggests that local freezing of water in the vicinity of hydrophobic species contributes to the experimental negative hydration enthalpy.

In the case of the methane sized hard sphere though, the hydration enthalpy at 298K is 5.0 kJ/mol, contrary to phenomenological expectations.

The Ostwald solubility is dictated by the ratio of the chemical potential and kT . The solubility of the methane sized solute in water as a function of temperature is shown in Fig. 6. This ratio passes through a maximum near 280K, corresponding to a minimum in the solubility. This observation is in agreement with information theory (Garde *et al.*, 1999) and equation-of-state (Ashbaugh *et al.*, 2002) models of HS solubilities that link the solubility minimum to the density maximum at 277K for pure water. The solubility minimum corresponds to the point at which the enthalpy, $h_S^{ex} = -T^2 \partial(\mu_S^{ex}/T)/\partial T|_{sat}$ equals zero. Real nonpolar solutes display solubility minimum at temperatures well above the density maximum, largely as a result of attractive interactions between the solute and water. These missing interactions can be included, albeit in an approximate manner, assuming they are proportional to the density of liquid water, as in the van der Waals equation-of-state. As a result the chemical potential can be written as $\mu_S^{ex} = \mu_S^{ex}|_{HS} - a_{SW}\rho_W$ (Garde *et al.*, 1999). The effect of including solute-water interactions on the solubility is shown in Fig. 6. Increasing these interactions systematically shifts the maximum in μ_S^{ex}/kT , out to greater temperatures, in agreement with the experimental observation of solubility minima at higher temperatures.

For the HS solutes that the simulation results have slightly more curvature at temperatures near the solubility minimum than predicted by Eq. 16-c (Fig. 6). While the fit is accurate, the enhanced curvature suggests the heat capacity is not constant as assumed above, but is slightly larger at low temperatures. Indeed this has been observed experimentally (Gill *et al.*, 1985), and is born out by theoretical models of hydrophobic hydration as well (Ashbaugh *et al.*, 2002; Hummer *et al.*, 2000; Silverstein *et al.*, 2001). Nevertheless, the temperature dependence of the heat capacity is minor and including it only complicates the interpretations here. We therefore neglect it in our thermodynamic analysis.

Fig. 7 shows the chemical potential density, $\mu_S^{ex}/\left(\frac{4\pi R^3}{3}\right)$, of hard cavities in water as a function of temperature with increasing solute size. In the range of sizes shown, the maximum in the chemical potential shifts from temperatures above 470K, above the window of temperatures simulated, for the 2Å radius solute to lower temperatures with increasing solute sizes. For cavities not much larger than 12Å (not shown in figure), the maximum falls below 260K, below the simulation window and the normal freezing point of water. Thus,

for molecularly sized cavities, hydrophobic hydration is opposed by a negative entropy, at temperatures below the chemical potential maximum, over most of the range of temperatures simulated. For meso- and macroscopic cavities, however, this trend is reversed and hydration is favored by a positive dissolution entropy but ultimately insoluble by an even larger positive enthalpy (demonstrated in the following section), as ultimately expected from the temperature dependence of the surface tension of water.

C. Surface area dependence of hydration thermodynamic properties: the Tolman length and curvature corrections

In an effort to compare and correlate hydration free energies of a variety species, it is common to calculate the free energy cost per unit area of hydrating nonpolar solute surfaces, also referred to as a molecular surface tension (Hermann, 1977; Tanford, 1979). This molecular surface tension, however, is generally not equal to the free energy of creating a macroscopic flat interface, in part due to solute curvature and structural differences between water at molecular and macroscopic interfaces. Nevertheless, SPT systematically interpolates the surface tension between these two length scale extremes and provides insight into their relationship (Ashbaugh and Paulaitis, 2001; Huang and Chandler, 2000).

Under the assumption that the pressure contribution to the hydration free energy is negligible, an excellent assumption for liquid water, the surface tension for hydrating a HS solute is determined by the surface area derivative of the chemical potential (Ashbaugh and Paulaitis, 2001). This derivative depends, however, on the definition of the solute surface area. A natural choice for the solute area is defined by R , and is referred to as the solvent accessible surface (SAS) area. Differentiating the chemical potential with respect to this surface yields

$$\gamma_{SAS}(R) = \frac{\partial \mu_S^{ex}}{\partial A} = \frac{\partial \mu_S^{ex}}{\partial 4\pi R^2} = \frac{1}{2}kT\rho_W G(R)R . \quad (17-a)$$

More generally, the solute surface can be defined by a radius $R - \Delta R$. In this case the surface tension is

$$\gamma_{\Delta R}(R) = \frac{\partial \mu_S^{ex}}{\partial [4\pi (R - \Delta R)^2]} = \frac{kT\rho_W G(R)R^2}{2(R - \Delta R)} = \frac{\gamma_{SAS}(R)}{1 - \Delta R/R} . \quad (17-b)$$

The SAS surface tension as a function of R at 300K is shown in Fig. 8. The surface enthalpy, $\partial h_0^{ex}/\partial A_{SAS}$, entropy, $\partial s_0^{ex}/\partial A_{SAS}$, and heat capacity, $\partial c_0^{ex}/\partial A_{SAS}$, are included

in this figure. For small cavities, all the surface thermodynamic properties go to zero as $R \rightarrow 0$. With increasing size, the surface tension increases monotonically and approaches its asymptotic limit for a flat interface of $\gamma_\infty = 0.432 \text{ kJ}/(\text{mol } \text{\AA}^2) = 71.7 \text{ dyne/cm}$. The other surface properties, particularly the heat capacity, approach their asymptotic plateaus more slowly with increasing R . Like the surface tension, the surface enthalpy monotonically increases with increasing solute size. The surface entropy and heat capacity, on the other hand, vary in distinctly different ways for molecular and macroscopic surfaces, indicating changes in the mechanism of hydration (Southall and Dill, 2000). In particular, the surface entropy is initially negative beginning from $R = 0$, consistent with the experimental thermodynamics of hydrophobic hydration for molecular solutes, reaches a minimum at $\approx 3.3 \text{\AA}$ and then increases, eventually becoming positive as expected from the temperature dependence of the liquid-vapor interface. It is curious that the size at this minimum is close to the size of the maximum of $G(R)$, that is for the *most hydrophobic* hard sphere solute. While the surface heat capacity is positive over the entire size range, it reaches a maximum at solute radii comparable to the position of the minimum in the entropy, suggesting the two are related.

Sharp and coworkers (Sharp *et al.*, 1991) suggested that rather than relying solely on the SAS to determine the molecular surface tension, this tension needs to be corrected for the curvature of the molecular interface to reconcile the difference between molecular and macroscopic surface tension. Based on geometric arguments, they proposed that the radius of a water molecule is the length scale over which this correction must be applied. In effect, their work indicates then that the van der Waals surface, i.e., $\Delta R = \sigma_{WW}/2 = 1.4 \text{\AA}$, provides a superior description of molecular solute hydration (Jackson and Sternberg, 1994; Sharp *et al.*, 1991). A schematic illustration of the van der Waals, solvent accessible, and curvature corrected radii of a hard sphere solute in water is given in Fig. 9. For a methane sized solute $\gamma_{SAS}(3.3 \text{\AA}) = 0.300 \text{ kJ}/(\text{mol } \text{\AA}^2)$, 30% lower than the macroscopic value, while $\gamma_{\Delta R=1.4 \text{\AA}} = 0.521 \text{ kJ}/(\text{mol } \text{\AA}^2)$, 20% greater than the macroscopic value. While neither of these two surfaces gives a surface free energy in agreement with the macroscopic limit, they do bracket γ_∞ suggesting there an optimal intermediate value of ΔR for which the surface tension is size independent. In Fig. 10 we show how the surface tension varies with increasing ΔR . The divergence in $\gamma_{\Delta R}$ results from the divergence in Eq. 17-b as $R \rightarrow \Delta R$. For solutes larger than 2.5\AA , using $\Delta R = 1 \text{\AA}$ yields a surface tension that is only weakly

dependent on size. Indeed, $\gamma_{\Delta R=1\text{\AA}}(3.3\text{\AA}) = 0.430 \text{ kJ}/(\text{mol \AA}^2)$ is in excellent agreement with the macroscopic value, suggesting that Honig and coworker's geometric estimate of the curvature correction length scale is essentially correct. This argument breaks down, however, when we consider the temperature dependence of the Tolman length.

Expanding the surface free energy in terms of surface curvature, (Tolman, 1949) derived the leading order curvature correction for the surface tension as

$$\gamma_{SAS} = \gamma_\infty \left(1 - \frac{2\delta}{R} \right) \quad (18\text{-a})$$

where δ is the Tolman length described above in the foundations of SPT. Substituting this expression into Eq. 17-b yields (Ashbaugh and Paulaitis, 2001)

$$\gamma_{\Delta R} = \gamma_\infty \left(\frac{1 - \frac{2\delta}{R}}{1 - \frac{\Delta R}{R}} \right) \quad (18\text{-b})$$

Thus, as a first approximation, the optimal surface for obtaining a size independent surface free energy is $\Delta R = 2\delta$. The Tolman length can be calculated from classic SPT, see Eq. 10 in Ref. 17, and yields an essentially temperature independent $\delta = 0.5 \text{ \AA}$ (Fig. 11), in good agreement with the empirical ΔR at 300K obtained above. The revised SPT, however, finds that δ has a significant temperature dependence (Fig. 11). While the classic SPT correctly predicts the magnitude of δ at low temperature, δ decreases with temperature and changes sign near 350K. Thus assuming ΔR is dictated by the size of a water molecule can lead to significant difficulties when interpreting the temperature dependence of microscopic surface tensions (Ashbaugh *et al.*, 1999; Jackson and Sternberg, 1994; Sharp *et al.*, 1991). In retrospect, the temperature dependence of the curvature correction may have been anticipated by the entropic differences between hydrating a molecular and mesoscopic interface and the significantly different temperature dependencies of the associated surface thermodynamic properties (Fig. 8). The curves observed in this figure are simply too rich to be described by a temperature independent length scale.

D. Entropy convergence and solute size

A feature of hydrophobic hydration believed to be shared between small molecule hydration and protein unfolding free energies is the phenomenon of entropy convergence. That is, when the hydrophobic component of the hydration entropies of these molecules is extrapol-

lated to high temperatures the entropies apparently converge to one another at a single temperature or narrow range of temperatures near 385K (Baldwin, 1986; Murphy *et al.*, 1990; Privalov, 1979; Privalov and Gill, 1988). Baldwin and Privalov have demonstrated this can result from the empirical suggestion that the entropy and heat capacity of hydration are proportional to one another. Perhaps the most successful explanations for the convergence temperature for small molecules have related the convergence temperature to the equation-of-state of pure water (Ashbaugh *et al.*, 2002; Garde and Ashbaugh, 2001; Hummer *et al.*, 1998). Still, Huang and Chandler have argued that for species greater than $\approx 10\text{\AA}$ in radius entropy convergence does not occur, and therefore proteins may not exhibit this phenomenon (Huang and Chandler, 2000).

In Fig. 12 we have plotted the hydration entropies for HS solutes as a function of temperature for solutes ranging in size from 2\AA to 10\AA in radius. Indeed, there is a broad range of convergence temperatures observed at each point where an entropy curve, for a given size, crosses that for another solute. For example, the 2\AA solute entropy intersects the 3\AA solute at 410K, while the 2\AA solute intersects the 10\AA solute curve at 300K, indicating that there is no unique convergence temperature. If we note, however, that entropy convergence studies have largely concerned themselves with solutes similar in size or at least of similar local curvature, e.g., the local curvature of an alkane is comparable to that of a constituent CH_2 group as far as water is concerned. We therefore consider how the convergence temperature changes with differential perturbations in the solute size. In this case, convergence occurs at the temperature for which $\Delta s_S^{ex} (R \rightarrow R + \delta R) = 0$. Assuming the hydration heat capacity is independent of temperature, T_c is determined by the relationship

$$T_c = T_0 \exp \left(-\frac{\partial s_0^{ex}}{\partial A_{SAS}} / \frac{\partial c_0^{ex}}{\partial A_{SAS}} \right) \quad (19)$$

with a size dependence dictated by the relationship between $\partial s_0^{ex} / \partial A_{SAS}$ and $\partial c_0^{ex} / \partial A_{SAS}$ on the solute radius in Fig. 8. The differential entropy convergence temperature curve determined by these expressions is shown in Fig. 12. Two points of interests are immediately apparent: first the convergence entropy is negative and becomes more negative with increasing solute size, second the convergence entropy curve more or less forms a lower bound on the hydration entropy as a function of temperature, although this behavior is not exact.

One of the implications of Eq. 19 is that if the entropy is a linear function of the heat capacity, *i.e.*, $s_0^{ex} = mc_0^{ex} + b$, as suggested by (Baldwin, 1986; Murphy *et al.*, 1990), then the

convergence temperature would be independent of solute size. In Fig. 13 we see that T_c has a significant solute size dependence, indicating this assumption is not generally correct or, at best, is valid only over limited circumstances of solute size. For solutes approaching zero radius, T_c plateaus at a maximum. With increasing solute size T_c decreases so that above a radius of $\approx 8\text{\AA}$ it is less than the normal freezing point of water. At the intermediate methane radius of 3.3\AA , however, the convergence temperature is 382K in excellent agreement with the experimental convergence temperature of 385K for simple nonpolar gases and linear alkanes.

We note that the convergence temperature as $R \rightarrow 0$ plateaus at 655K, above the critical temperature of water at 647K. This unphysical result is due, in part, to our extrapolation of the entropies beyond the range, 260K to 470K, to which we fitted Eq. 16-c. For cavities for which only one water molecule can fit inside so that the free energy is determined by Eq. 6, entropy convergence is determined as the temperature at which

$$T_c = \frac{1 - \frac{4\pi}{3}R^3\rho_W}{\alpha_{sat}} \quad (20)$$

is satisfied, where $\alpha_{sat} = -\partial\rho_W/\partial T$ is the thermal expansion coefficient of liquid water along the saturation curve. When this criteria is applied, it displays a plateau at a physically more realistic temperature of $T_c \approx 525\text{K}$ (Fig. 13). With increasing solute size, Eq. 20 indicates a sudden decrease in T_c above radii of $\approx 1\text{\AA}$, comparable to what was observed assuming the heat capacity is temperature independent. Above radii of 1.25\AA , Eq. 20 breaks down as multi-particle correlations began to play a role in the solute entropy. At this radius, however, the convergence temperatures are now within the range of temperatures simulated and the application of Eq. 19 becomes more accurate. It is reasonable then to interpolate between the convergence temperatures determined by eqs. 19 and 20, as indicated in Fig. 13. We note that information theory, under reasonable assumptions for liquid water, suggests that entropy convergence occurs when $T_c = (2\alpha_{sat})^{-1}$ (Garde *et al.*, 1996; Hummer *et al.*, 1998). This criteria is satisfied at 420K, corresponding to a solute radius of $\approx 2.1\text{\AA}$ on Fig. 13, decidedly placing IT among small solute theories. Relaxing the assumptions used to arrive at the IT criteria lowers the convergence temperature prediction for methane sized solutes to $\approx 390\text{K}$, in markedly improved agreement with the present result of 382K.

The apparent convergence of the entropy change at 385K to a value close to zero for a range of hydrophobic solutes and proteins has suggested empirically that the hydration of

these chemically distinct solutes are related (Baldwin, 1986; Murphy *et al.*, 1990). Assuming that the temperature dependence for protein unfolding arises solely from the exposure of hydrophobic side chains to water, phenomenological models have been developed which separate out residual temperature independent components of the entropy, from contributions such as changes in the chain conformation, by extrapolating to the convergence temperature. This procedure relies, in part, on the assumption that the hydration of surface hydrophobic groups is the same in the native and denatured conformations, and therefore cancels in the entropy difference.

Huang and Chandler (Huang and Chandler, 2000) suggested that the hydration of surface nonpolar groups is better described by the hydration entropy of a solute surface comparable in size to the protein radius on the order of tens of angstroms, rather than treating the surface groups individually as having sizes comparable to simple hydrophobic units. In this case, the hydration entropy of the surface groups depends on the protein conformation and the difference between folded and unfolded states is not negligible, as illustrated by the differences between the hydration entropies for HS solutes of differing size in Fig. 12. This hypothesis presumes that entropic contributions for hydrating large hydrophobic surfaces with attractive dispersion interactions and vicinal polar/charged groups is the same as that for a hard repulsive surface. Recent simulations of convex methane clusters have found that when realistic attractive interactions between water and methane are included, water packs around the cluster methane sites just as it does around a solitary methane in solution (Ashbaugh and Paulaitis, 2001). Moreover, Cheng and Rossky (Cheng and Rossky, 1998) found that the orientational correlations between water and proximal hydrophobic residues on the convex surfaces of the bee venom protein, meletin, are comparable to those near individual solitary hydrophobic groups in solution. These observations suggest that the available configurational space, and by extension the entropy, for waters near realistic surface hydrophobic units is the same in the folded and unfolded states, supporting the assumptions of the phenomenological folding models. We note, however, that in the same study Cheng and Rossky found that waters proximal to hydrophobic residues in flat portions of meletin were more orientationally disordered as a result of the difficulties associated with maintaining the aqueous hydrogen-bonding network near restrictive solute topologies.(Cheng and Rossky, 1998) Thus, the applicability of the phenomenological unfolding model may be complicated by the protein surface topography and the impact of

hydrophobic pockets on the overall unfolding entropy. As a result, scatter can be introduced into folding entropies as determined by calorimetric studies (Robertson and Murphy, 1997).

IV. SUMMARY AND CONCLUSIONS

The revised scaled particle theory (SPT) proposed here, which extends Stillinger's SPT (Stillinger, 1973), utilizes information on multi-body correlations in liquid water, interrogated with detailed molecular simulations, and experimental information (the macroscopic liquid-vapor surface tension and the saturation pressure of water) to construct a functional form for the hydration free energy of hard sphere (HS) model hydrophobic solutes that successfully bridges the known molecular and macroscopic limits. Most notably, the revised SPT provides a more accurate representation of the contact correlation function in aqueous solution, central to scaled particle calculations, than predicted by the classic SPT expressions extracted from the basic theory Reiss for the hard sphere fluid. Relying on classic SPT for predictions of HS hydration free energies results in a number of suspicious conclusions, including an unphysical increase in the surface tension of water with increasing temperature and a temperature independent Tolman length, which do not agree with experimental or revised SPT observations. As a result, application of classic SPT to hydration free energies is largely a fitting exercise to obtain the effective HS diameter of water, and conclusions drawn have weak significance regarding the molecular origins of the hydrophobic effect.

The revised SPT is more successful, but the success of the scaled particle approach generally derives from the remarkable fact that the results sharply identify a molecular length scale, near 3.0\AA , that provides a good joining point for microscopic and macroscopic descriptions. It could have been otherwise, and the corresponding results are less simple in the cases of comparative organic solvents (Graziano, 2003; Pratt and Pohorille, 1992). That micro-macro boundary length does exhibit interesting, non-simple temperature variation; an accurate description of those temperature variations is an important part of the higher fidelity of the revised scaled particle results. The revised SPT does reproduce the well documented solubility minimum behavior for small hydrophobic solutes and demonstrates significant changes in the hydration mechanism of HS solutes with increasing solute size. In particular, while the hydration thermodynamics of small solutes is predominantly entropic in origin at room temperature, the hydration of mesoscopic cavities is entropically favorable and

opposed by a dominating hydration enthalpy. While it is tempting to describe these changes in hydration thermodynamic quantities in terms of aqueous hydrogen-bonding near the hydrophobic entity — and that may be plausible sometimes — the SPT provides little in the way of information on the integrity of bonded networks. Nevertheless the revised SPT does provide thermodynamic information that challenges phenomenological views of hydrophobic effects, particularly the cherished *iceberg* hypothesis. Indeed, the iceberg hypothesis suggests that local freezing of water molecules in the vicinity of hydrophobic solutes is a source for the negative hydration enthalpies, we find that at room temperature the hydration of solutes comparable in size to methane and a number of nonpolar gases is actually unfavorable from an enthalpic as well as an entropic standpoint.

Attempts to reconcile the differences between molecular and macroscopic values of the surface tension suggest that on a molecular level there is a unique surface that maps macroscopic surface tensions to molecular values. This reduces the reconciliation to the program of finding the appropriate dividing surface. The utility of that program rests on the optimistic expectation that the Tolman length might be only weakly dependent on temperature. Although there is some support for that expectation from classic SPT, the revised SPT model demonstrates that the Tolman length has a significant temperature dependence in water, changing signs from positive to negative at $\approx 350\text{K}$. Indeed, that possibility was put forth by Stillinger (Stillinger, 1973). As a result then, while the optimal surface for the description of hydration may be approximated by the solute van der Waals surface at low temperatures (Ashbaugh *et al.*, 1999; Ashbaugh and Paulaitis, 2001), with increasing temperature this optimized surface moves out to the solvent accessible surface at $\approx 350\text{K}$ and ultimately extends beyond this surface at even higher temperatures as a result of the nontrivial temperature dependencies to the hydration thermodynamics of molecular sized solutes.

Finally, the revised SPT provides detailed information on the curious entropy convergence behavior observed for small molecular solutes and nonpolar gases and the size dependence of the convergence temperature on increasing size. While Huang and Chandler have cited the eclipsing of the convergence temperature below the freezing temperature of water for large, protein-sized, cavities as the source for scatter in the convergence temperature in the analysis of protein unfolding thermodynamic data, the SPT analysis suggests that even the moderate differences in hydrophobic amino acid side chain sizes is sufficient to scatter the results of unfolding thermodynamics. While the treatment of small hydrophobic species as

an effective HS is justifiable, a similar extension to mesoscopic assemblies may be doubtful. Indeed, simulation analyses of the structure of water near proteins and hydrophobic clusters suggest that it bears resemblances to the hydration structure near the constituent amino acids (Ashbaugh and Paulaitis, 2001; Cheng and Rossky, 1998). A primary difficulty in the interpretation of assembly processes is that the hydration of amphiphilic species is complex and distinct contributions may not be individually separable. That is to say, local context matters.

Acknowledgements

This work was supported by the U. S. Department of Energy, contract E-7405-ENG-36. HSA gratefully acknowledges support from a Los Alamos Director's Fellowship. This research has benefited from conversations with Andrew Pohrille, Angel García, Gerhard Hummer, Shekhar Garde, Dilipkumar Asthagiri, and Michael Paulaitis.

References

Alejandre, J., D. J. Tildesley, and G. A. Chapela, 1995, *J. Chem. Phys.* **102**, 4574.

Ashbaugh, H. S., D. Asthagiri, L. R. Pratt, and S. B. Rempe, 2003, *Biophys. Chem.* In press.

Ashbaugh, H. S., E. W. Kaler, and M. E. Paulaitis, 1999, *J. Am. Chem. Soc.* **121**, 9243.

Ashbaugh, H. S., and M. E. Paulaitis, 1996, *J. Phys. Chem.* **100**, 1900.

Ashbaugh, H. S., and M. E. Paulaitis, 2001, *J. Am. Chem. Soc.* **123**, 10721 .

Ashbaugh, H. S., T. M. Truskett, and P. G. Debenedetti, 2002, *J. Chem. Phys.* **116**, 2907.

Baldwin, R. L., 1986, *Proc. Natl. Acad. Sci. USA* **83**, 8069.

Ben-Naim, A., and Y. Marcus, 1984, *J. Chem. Phys.* **81**, 2016 .

Berendsen, H. J. C., J. R. Grigera, and T. P. Straatsma, 1987, *J. Phys. Chem.* **91**, 6269 .

Blokzijl, W., and J. B. F. N. Engberts, 1993, *Angew. Chem. Int. Ed. Engl.* **32**, 1545.

Bowron, D. T., A. Filippioni, C. Lobban, and J. L. Finney, 1998a, *Chem. Phys. Letts.* **293**, 33.

Bowron, D. T., A. Filippioni, M. A. Roberts, and J. L. Finney, 1998b, *Phys. Rev. Lett.* **81**, 4164 .

Brandts, J. F., 1964, *J. Am. Chem. Soc.* **86**, 4291.

Broadbent, R. D., and G. W. Neilson, 1994, *J. Chem. Phys.* **100**, 7543 .

Chandler, D., 1993, *Phys. Rev. E* **48**, 2898 .

Chen, L. J., S. Y. Lin, and C. C. Huang, 1998a, *J. Phys. Chem. B* **102**, 4350.

Chen, L. J., S. Y. Lin, C. C. Huang, and E. M. Chen, 1998b, *Colloids Surf. A* **135**, 175 .

Cheng, Y. K., and P. J. Rossky, 1998, *Nature* **392**, 696.

Christenson, H. K., and P. M. Claesson, 1988, *Science* **239**, 390 .

Considine, R. F., R. A. Hayes, and R. G. Horn, 1999, *Langmuir* **15**, 1657 .

DeJong, P. H. K., J. E. Wilson, G. W. Neilson, and A. D. Buckingham, 1997, *Molecular Physics* **91**, 99.

Filipponi, A., D. T. Bowron, C. Lobban, and J. L. Finney, 1997, *Phys. Rev. Letts.* **79**, 1293.

Frank, H. S., and M. W. Evans, 1945, *J. Chem. Phys.* **13**, 507.

Franks, F., and R. H. M. Hatley, 1991, *Pure Appl. Chem.* **63**, 1367.

Frenkel, D., and B. Smit, 2002, *Understanding Molecular Simulation. From Algorithms to Applications* (Academic Press, San Diego), 2nd edition.

Garde, S., and H. S. Ashbaugh, 2001, *J. Chem. Phys.* **115**, 977.

Garde, S., A. E. García, L. R. Pratt, and G. Hummer, 1999, *Biophys. Chem.* **78**, 21.

Garde, S., G. Hummer, A. E. García, M. E. Paulaitis, and L. R. Pratt, 1996, *Phys. Rev. Letts.* **77**, 4966.

Gill, S. J., S. F. Dec, G. Olofsson, and I. Wadso, 1985, *J. Phys. Chem.* **89**, 3758 .

Graziano, G., 2003, *Biophys. Chem.* **104**, 393 .

Henderson, J. R., 2002, *J. Chem. Phys.* **116**, 5039 .

Hermann, R. B., 1977, *Proc. Natl. Acad. Sci. USA* **74**, 4144 .

Huang, D. M., and D. Chandler, 2000, *Phys. Rev. E* **61**, 1501.

Hummer, G., and S. Garde, 1998, *Phys. Rev. Letts.* **80**, 4193.

Hummer, G., S. Garde, A. E. Garcia, M. E. Paulaitis, and L. R. Pratt, 1998, *J. Phys. Chem. B* **102**, 10469.

Hummer, G., S. Garde, A. E. Garcia, A. Pohorille, and L. R. Pratt, 1996, *Proc. Natl. Acad. Sci. USA* **93**, 8951 .

Hummer, G., S. Garde, A. E. Garcia, and L. R. Pratt, 2000, *Chem. Phys.* **258**, 349.

Hura, G., D. Russo, R. M. Glaeser, T. Head-Gordon, M. Krack, and M. Parrinello, 2003, *Phys. Chem. Chem. Phys.* **5**, 1981 .

Israelachvili, J., and R. Pashley, 1982, *Nature* **300**, 341.

Jackson, R. M., and M. J. E. Sternberg, 1994, *Prot. Eng.* **7**, 371 .

Kauzmann, W., 1959, *Adv. Protein Chem.* **14**, 1.

Kokkoli, E., and C. F. Zukoski, 1998, *Langmuir* **14**, 1189.

Lazaridis, T., 2001, *Acc. Chem. Res.* **34**, 931.

Lazaridis, T., and M. E. Paulaitis, 1992, *J. Phys. Chem.* **96**, 3847.

Lee, B., 1985, *Biopolymers* **24**, 813.

Lee, B., 1991, *Proc. Natl. Acad. Sci. USA* **88**, 5154 .

Lum, K., D. Chandler, and J. D. Weeks, 1999, *J. Phys. Chem. B* **103**, 4570.

Makhatadze, G. I., and P. L. Privalov, 1995, *Adv. Protein Chem.* **47**, 307 .

Muller, N., 1993, *Biopolymers* **33**, 1185 .

Murphy, K. P., P. L. Privalov, and S. J. Gill, 1990, *Science* **247**, 559.

Pashley, R. M., 2003, *J. Phys. Chem. B* **107**, 1714 .

Pashley, R. M., P. M. McGuiggan, B. W. Ninham, and D. F. Evans, 1985, *Science* **229**, 1088.

Pierotti, R. A., 1976, *Chem. Rev.* **76**, 717.

Pohorille, A., and L. R. Pratt, 1990, *J. Am. Chem. Soc.* **112**, 5066.

Pollack, G. L., 1991, *Science* **251**, 1323.

Pratt, L., G. Hummer, and S. Garde, 1999, in *New Approaches to Problems in Liquid State Theory*, edited by C. Caccamo, J.-P. Hansen, and G. Stell (Kluwer, Netherlands), volume NATO Science Series 529, pp. 407–420.

Pratt, L. R., 1998, in *Encyclopedia of Computational Chemistry* (John Wiley & Sons, Chichester), pp. 1286–1294.

Pratt, L. R., 2002, *Annu. Rev. Phys. Chem.* **53**, 409.

Pratt, L. R., and D. Chandler, 1977, *J. Chem. Phys.* **67**, 3863.

Pratt, L. R., and A. Pohorille, 1992, *Proc. Natl. Acad. Sci. USA* **89**, 2995.

Pratt, L. R., and A. Pohorille, 1993, in *Proceedings of the EBSA 1992 International Workshop on Water-Biomolecule Interactions*, edited by M. U. Palma, M. B. Palma-Vittorelli, and F. Parak (Societá Italiana de Fisica, Bologna), pp. 261–268.

Privalov, P. L., 1979, *Adv. Prot. Chem.* **33**, 167.

Privalov, P. L., and S. J. Gill, 1988, *Adv. Prot. Chem.* **39**, 191 .

Reiss, H., 1965, *Adv. Chem. Phys.* **9**, 1.

Reiss, H., 1977, in *Statistical Mechanics and Statistical Methods in Theory and Application*, edited by U. Landman (Plenum, New York), pp. 99–138.

Reiss, H., H. L. Frisch, and J. L. Lebowitz, 1959, J. Chem. Phys. **31**, 369.

Robertson, A. D., and K. P. Murphy, 1997, Chem. Rev. **97**, 1251.

Scatena, L. F., M. G. Brown, and G. L. Richmond, 2001, Science **292**, 908.

Sharp, K. A., A. Nichols, R. F. Fine, and B. Honig, 1991, Science **252**, 106.

Silverstein, K. A. T., K. A. Dill, and A. D. J. Haymet, 2001, J. Chem. Phys. **114**, 6303.

Simonson, T., 2003, Rep. Prog. Phys. **66**, 737 .

Southall, N. T., and K. A. Dill, 2000, J. Phys. Chem. B **104**, 1326 .

Stillinger, F. H., 1973, J. Soln. Chem. **2**, 141.

Stillinger, F. H., and M. A. Cotter, 1971, J. Chem. Phys. **55**, 3449.

Tanford, C., 1979, Proc. Nat. Acad. Sci. USA **76**, 4175.

Tanford, C., 1980, *The Hydrophobic Effect: Formation of Micelles and Biological Membranes* (John Wiley & Sons, New York), 2nd edition.

Tolman, R. C., 1949, J. Chem. Phys. **17**, 333 .

Truskett, T. M., P. G. Debenedetti, and S. Torquato, 2001, J. Chem. Phys. **114**, 2401.

Weeks, J. D., K. Katsov, and K. Vollmayr, 1998, Phys. Rev. Letts. **81**, 4400.

Widom, B., 1982, J. Phys. Chem. **86**, 869.

Figures

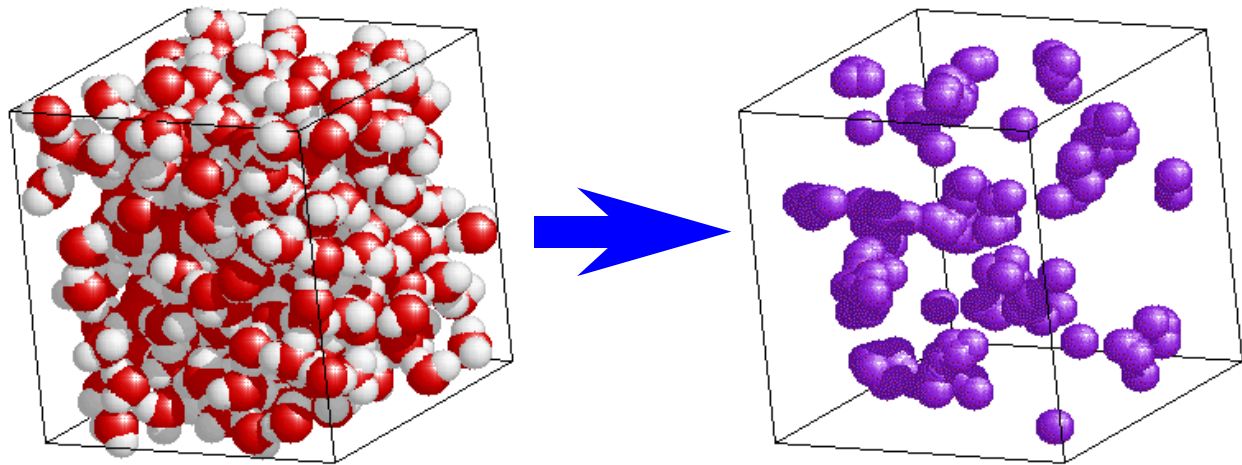


FIG. 1 Available volume for a 3\AA hard sphere in a simulation box of water. The box on the left shows a configuration of water taken from a simulation at 300 K. The box on the right shows the volume available to a 3\AA hard sphere cavity in that same water configuration.

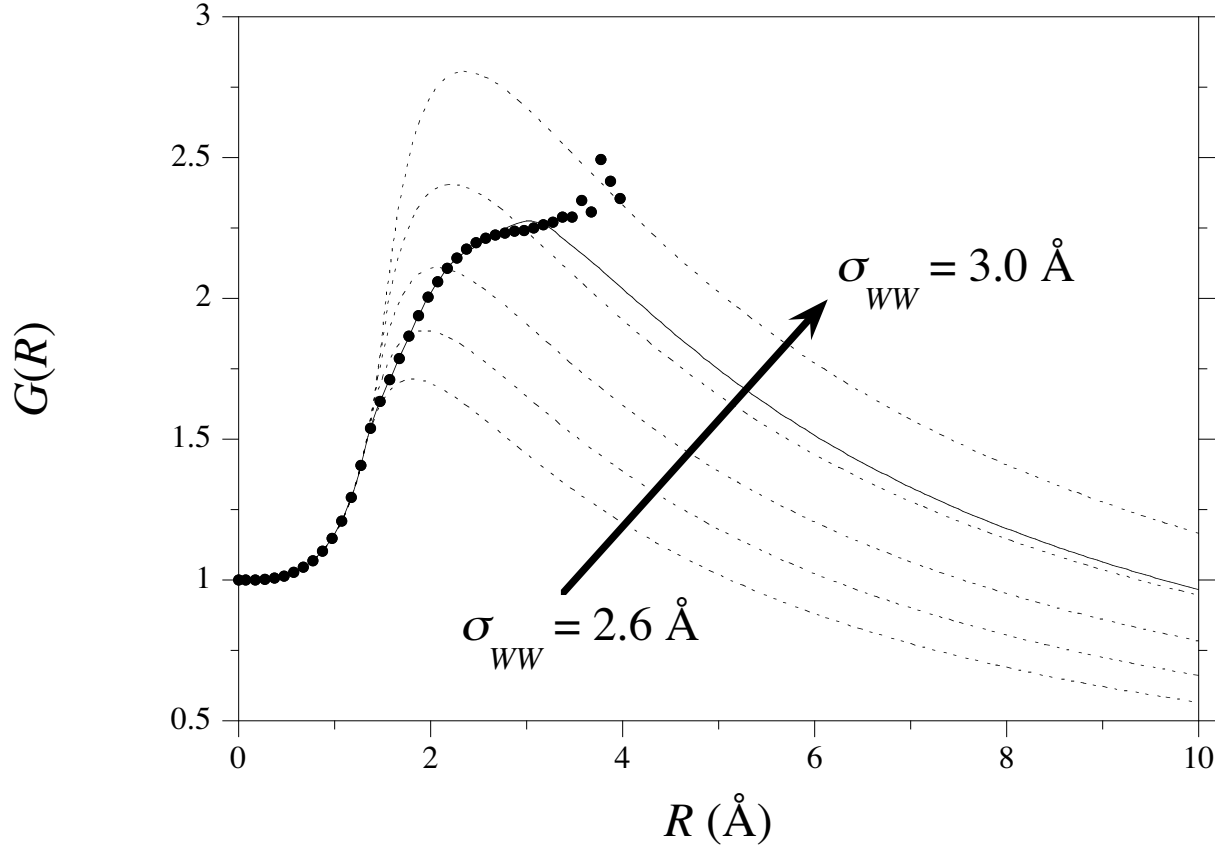


FIG. 2 Cavity contact correlation function for water at 300K at the liquid saturation conditions. The points are obtained by differentiation of the simulation cavity insertion probabilities. The dashed lines are obtained from Reiss's original SPT theory predictions for a hard sphere solvent, Eq. 10, using effective water hard sphere diameters between $\sigma_{WW} = 2.6 \text{ \AA}$ to 3.0 \AA in 0.1 \AA increments. The solid line is obtained by differentiation of the revised SPT, Eq. 15, fitted to the simulation results between $R_{sim} = 2.5 \text{ \AA}$ and $R_{macro} = 3.5 \text{ \AA}$.

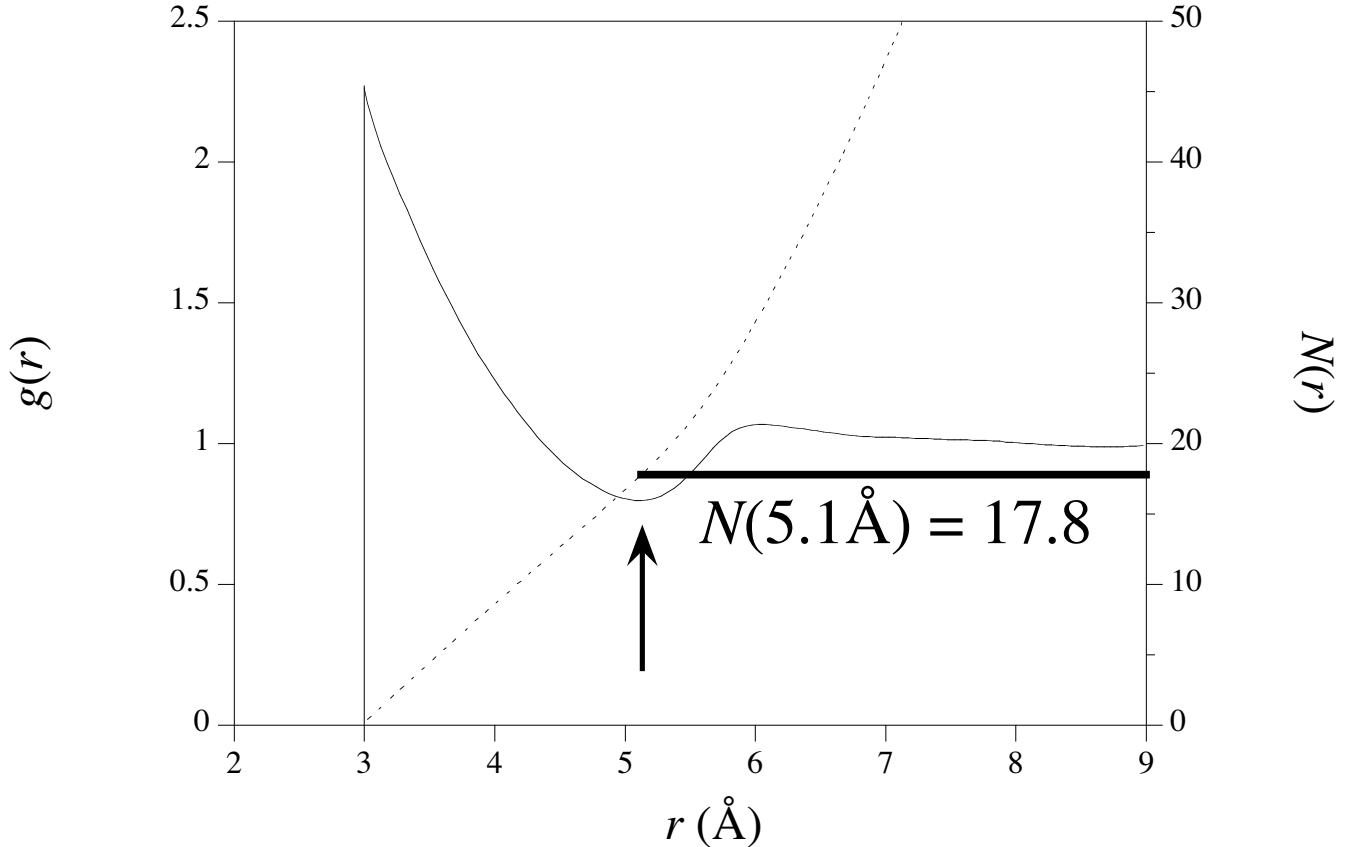


FIG. 3 Cavity-water oxygen radial distribution function for a 3 Å cavity at 300K. The thin solid line indicates the radial distribution function, while the dashed line indicates the radial integral $N(r) = \int_0^r \rho_W g(\lambda) 4\pi \lambda^2 d\lambda$. The occupation of the first hydration shell, corresponding to the first minimum in $g(r)$ at 5.1 Å, is 17.8 water molecules as indicated by the thick horizontal line. Note that the first minimum, which physically discriminates between first and succeeding hydration shells, is mild, and structuring of outer hydration shells is weak (Pratt and Pohorille, 1993). These features are in good qualitative agreement with the predictions of the Pratt-Chandler theory (Pratt and Chandler, 1977), though that limited theory has been substantially amended (Pratt, 2002).

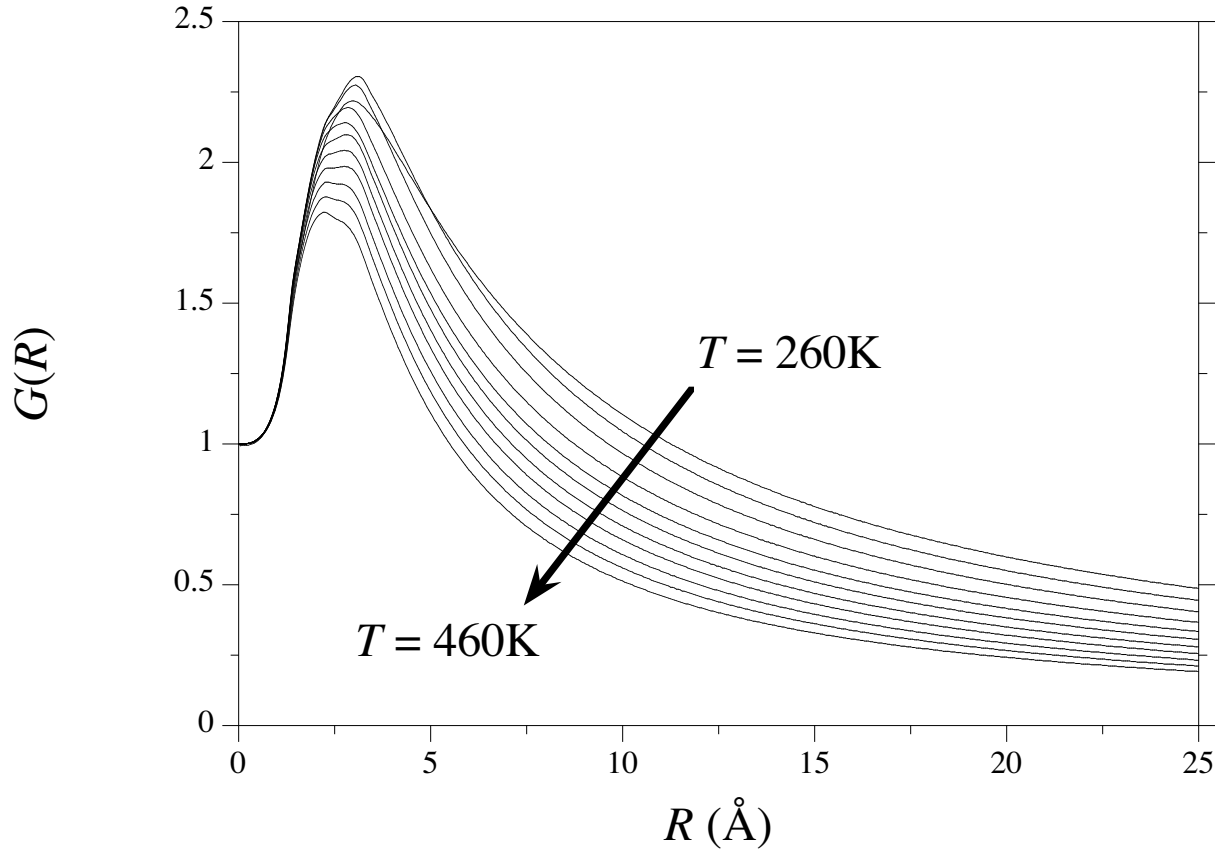


FIG. 4 Cavity contact function for water as a function of temperature along the liquid saturation curve determined by the revised SPT, Eq. 14, with $R_{sim} = 2.5\text{\AA}$ and $R_{macro} = 3.5\text{\AA}$. Results are shown between 260K to 460K in 20K increments. Notice that the length defined by the maximum of this curve *decreases* with decreasing density following increasing temperature along the saturation curve.

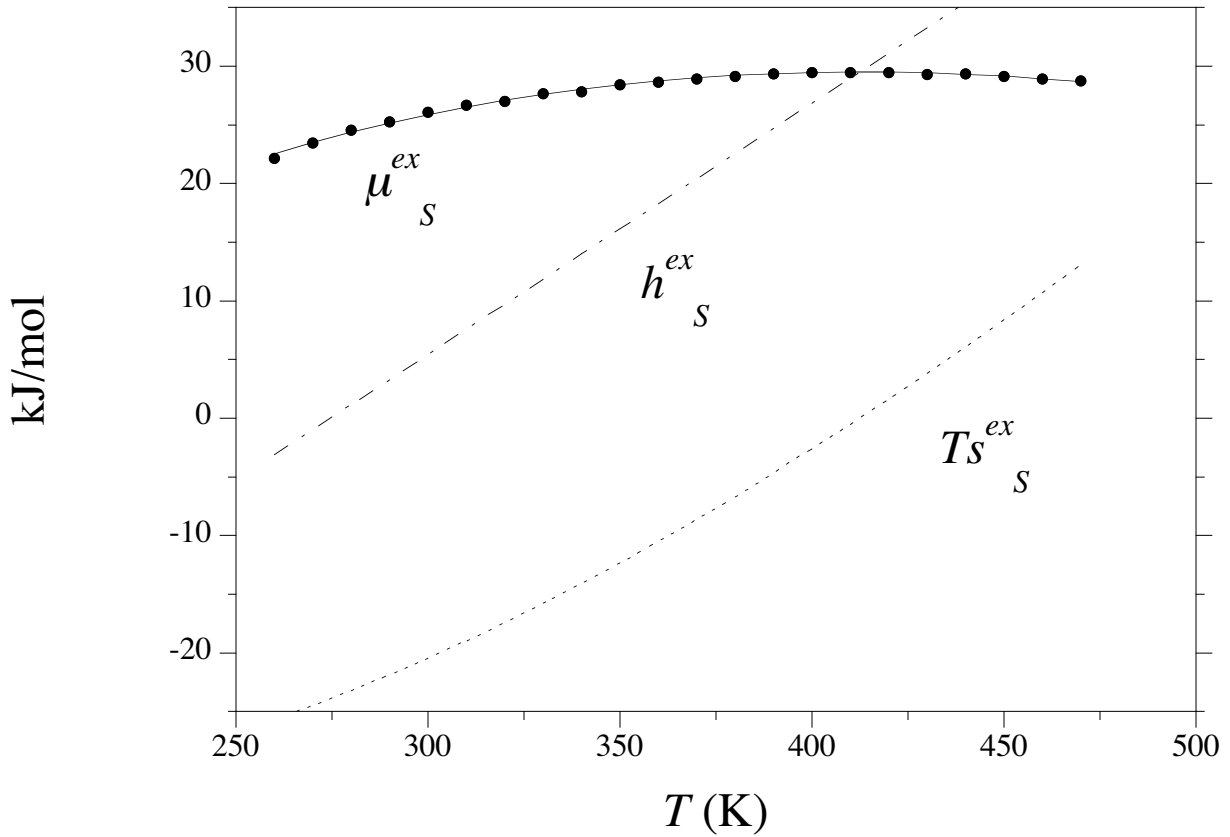


FIG. 5 Excess chemical potential, enthalpy, and entropy of a methane sized hard sphere solute ($R = 3.3\text{\AA}$) in water as a function of temperature along the saturation curve. The points are the explicit simulation results for the chemical potential. Error bars are comparable in size to the points. The curves for the excess chemical potential, enthalpy, and entropy are labeled in the figure. The curves were determined under the assumption that the heat capacity is independent of temperature (Eqs. 16).

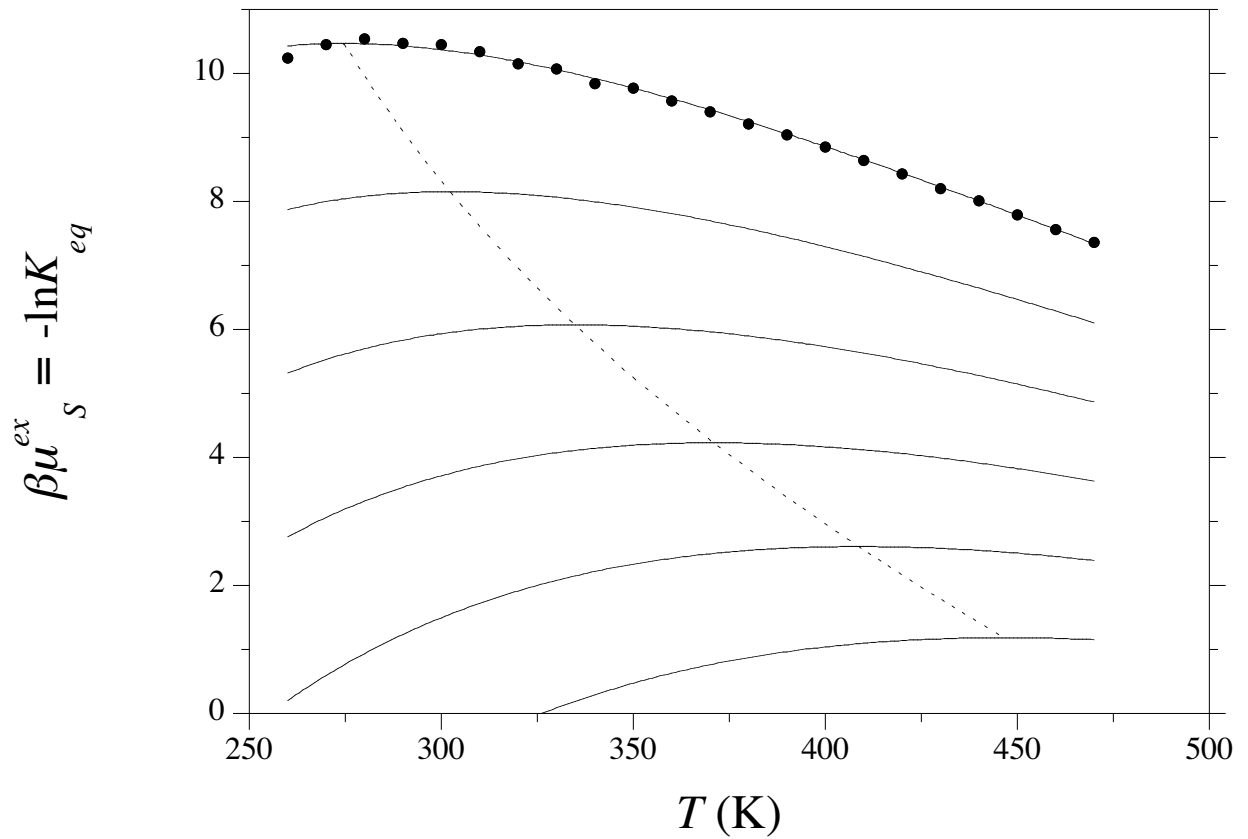


FIG. 6 Solubility of a 3.3\AA HS solute with increasing attractive interactions as a function of temperature. The points are simulation results from particle insertion probabilities. The solid curves are the solubilities with lower curves indicating increasing attractive interactions, a_{SW} . The dashed curve indicates the maxima in μ_S^{ex}/kT with increasing interactions, corresponding to minima in the Ostwald solubility.

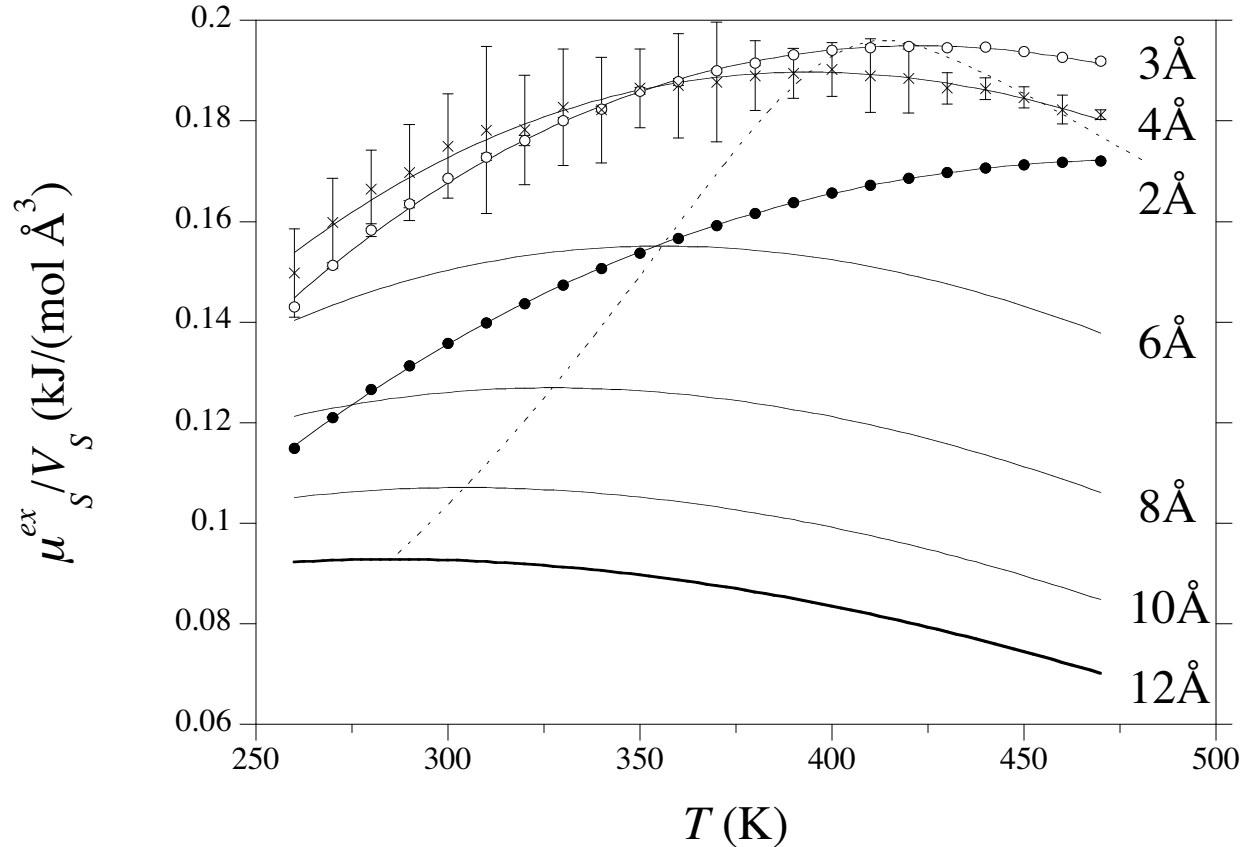


FIG. 7 Excess solute chemical potential density ($V_S = \frac{4\pi R^3}{3}$) as a function of temperature for solutes of varying size. The solid lines correspond to the revised SPT model. The solid circles, open circles, and crosses correspond to explicit molecular simulation results simulation results for the 2\text{\AA}, 3\text{\AA}, and 4\text{\AA} radius solutes, respectively. The error bars, greatest for the 4\text{\AA} cavity, indicate one standard deviation. The dashed line indicates the locus of chemical potential maxima, where $s_S^{ex} t = 0$, with changing cavity size.

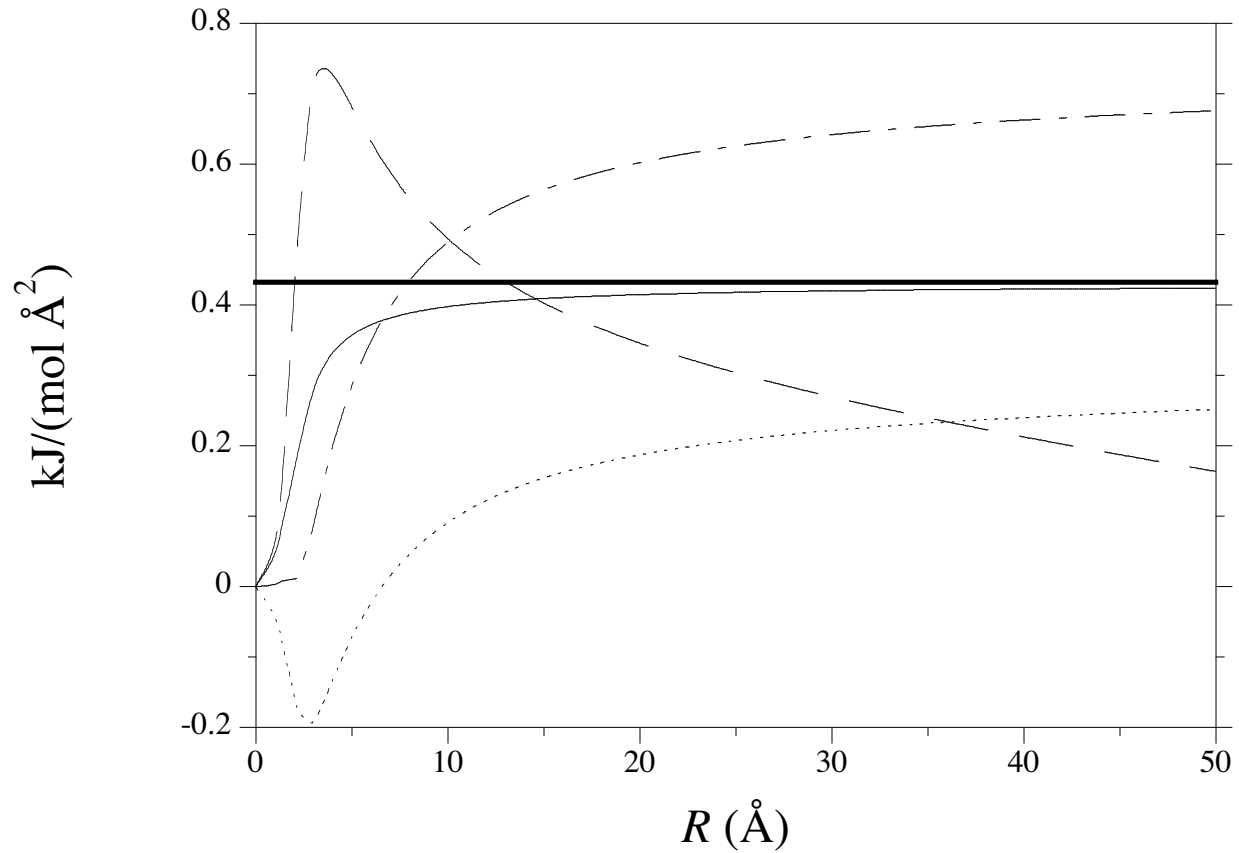


FIG. 8 HS solvent accessible surface area derivatives of the thermodynamic variables as a function of solute radius at $T_0 = 300\text{K}$. The thin solid, long-short dashed, and short dashed, and long dashed lines correspond to $\partial\mu_S^{ex}/\partial A$, $\partial h_S^{ex}/\partial A$, $T\partial s_S^{ex}/\partial A$, $T\partial c_S^{ex}/\partial A$, respectively. The thick horizontal line indicates the macroscopic surface tension for a flat surface.

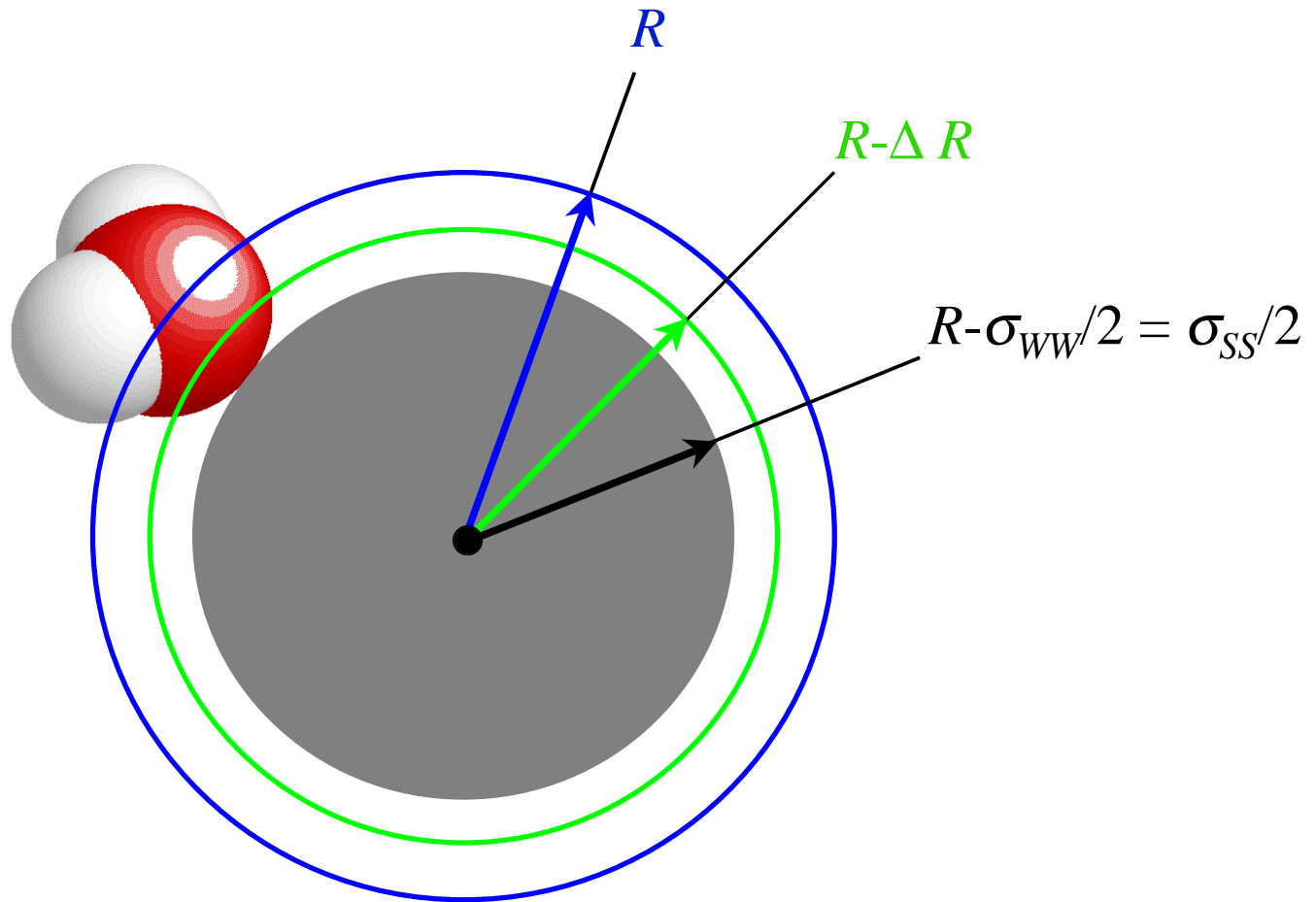


FIG. 9 Alternative definitions of the radius of a hard sphere cavity. The solvent accessible radius, R , is given by the distance of closest approach between the center of the cavity and the water oxygen center. The radius $R - \sigma_{WW}/2$ demarks the van der Waals boundary of the cavity at $\sigma_{SS}/2$. $R - \Delta R$ denotes the surface tension curvature corrected radius.

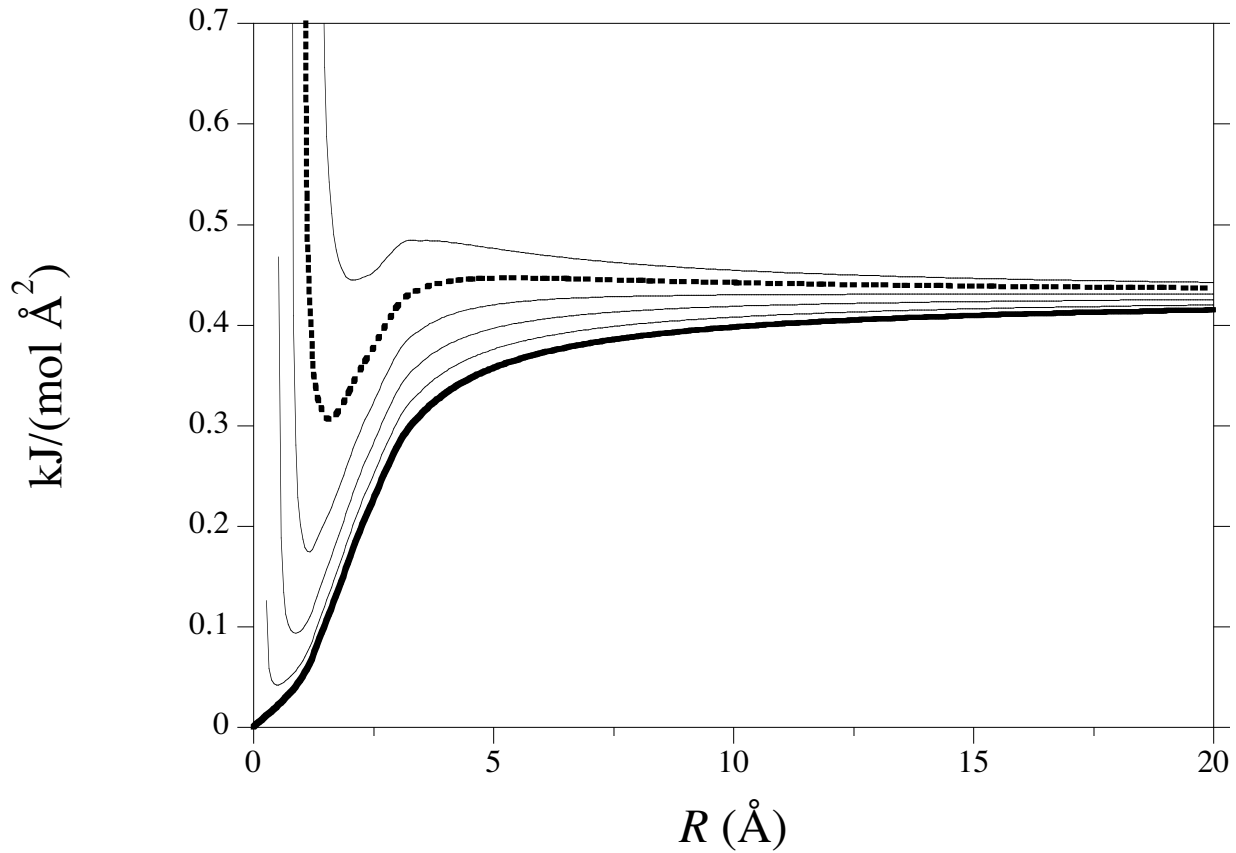


FIG. 10 Surface tension of HS hydration in water as a function of solute radius at 300K employing different definitions of the solute surface. The thick solid line corresponds to the surface tension determined by the derivative with respect to the solvent accessible surface area defined by the radius R (Eq. 17-a). The lines above the baseline SAS surface tension indicate the effect of increasing ΔR in 0.25\AA increments from 0.25\AA to 1.25\AA (Eq. 17-b). The thick dashed line corresponds to $\Delta R = 1\text{\AA}$.

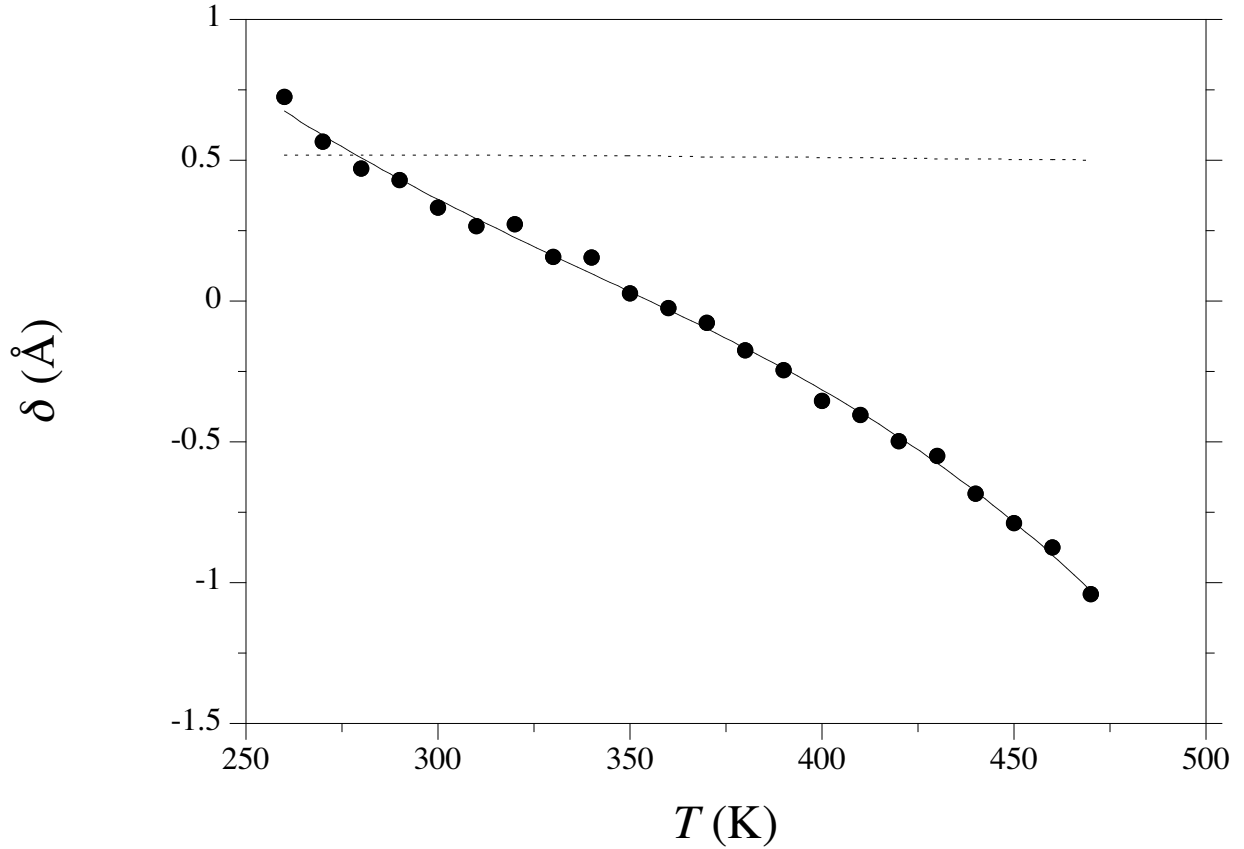


FIG. 11 Tolman length, δ , as a function of temperature along the saturation curve of water. The points correspond to the values determined by the fit of Eq. 14 to the simulation free energies. The solid line is a guide to the eye for the fitted results. The dashed line corresponds to the classic SPT prediction for the Tolman length, Eq. 10 in ref. 17.

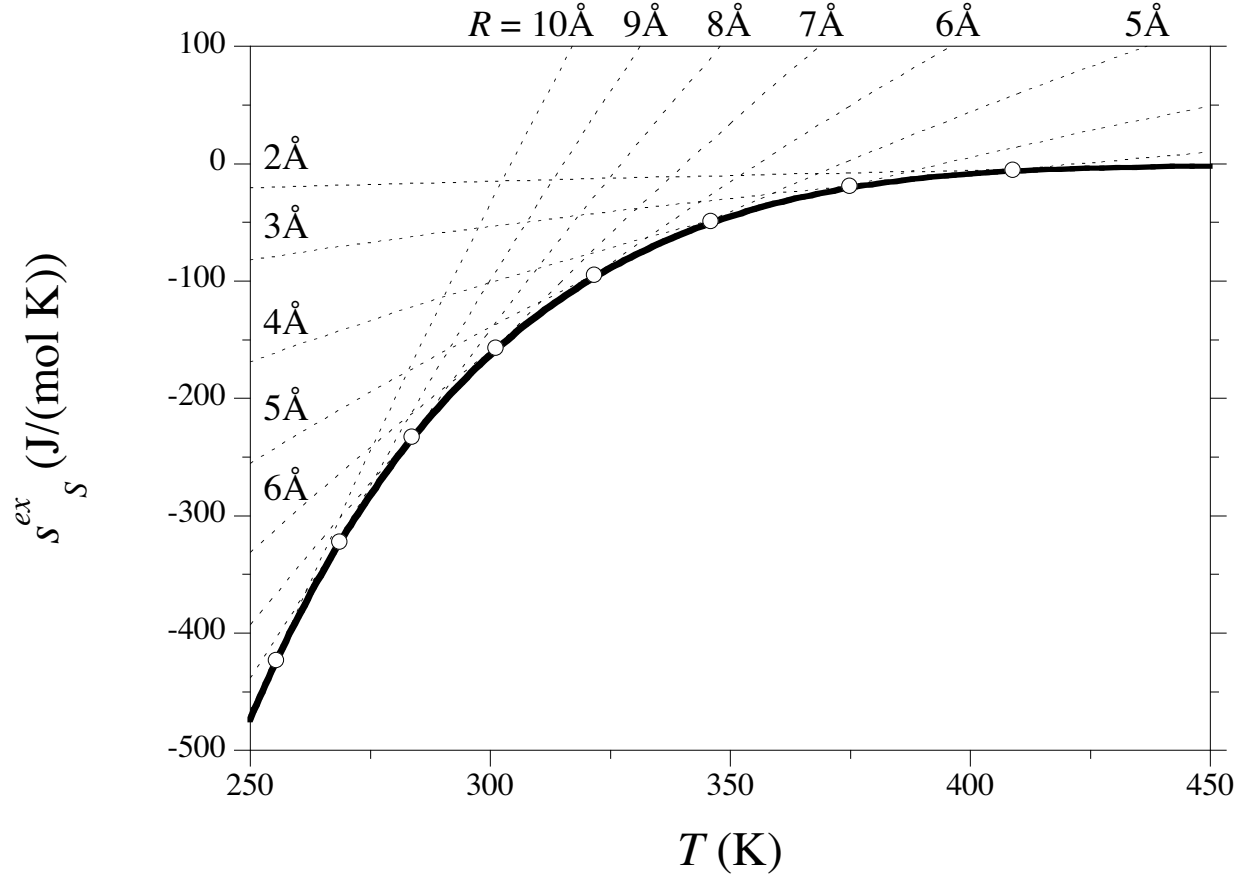


FIG. 12 Entropy of hydrophobic hydration as a function of temperature for solutes ranging in radius from 2\AA to 10\AA in 1\AA increments. The dashed lines are the excess entropies of hydration. The open circles are the convergence temperatures for consecutive solutes, *i.e.*, $s_S^{ex}(R) = s_S^*(R+1\text{\AA})$. The thick solid line indicates the entropy convergence temperature in the limit of infinitesimal perturbations in R .

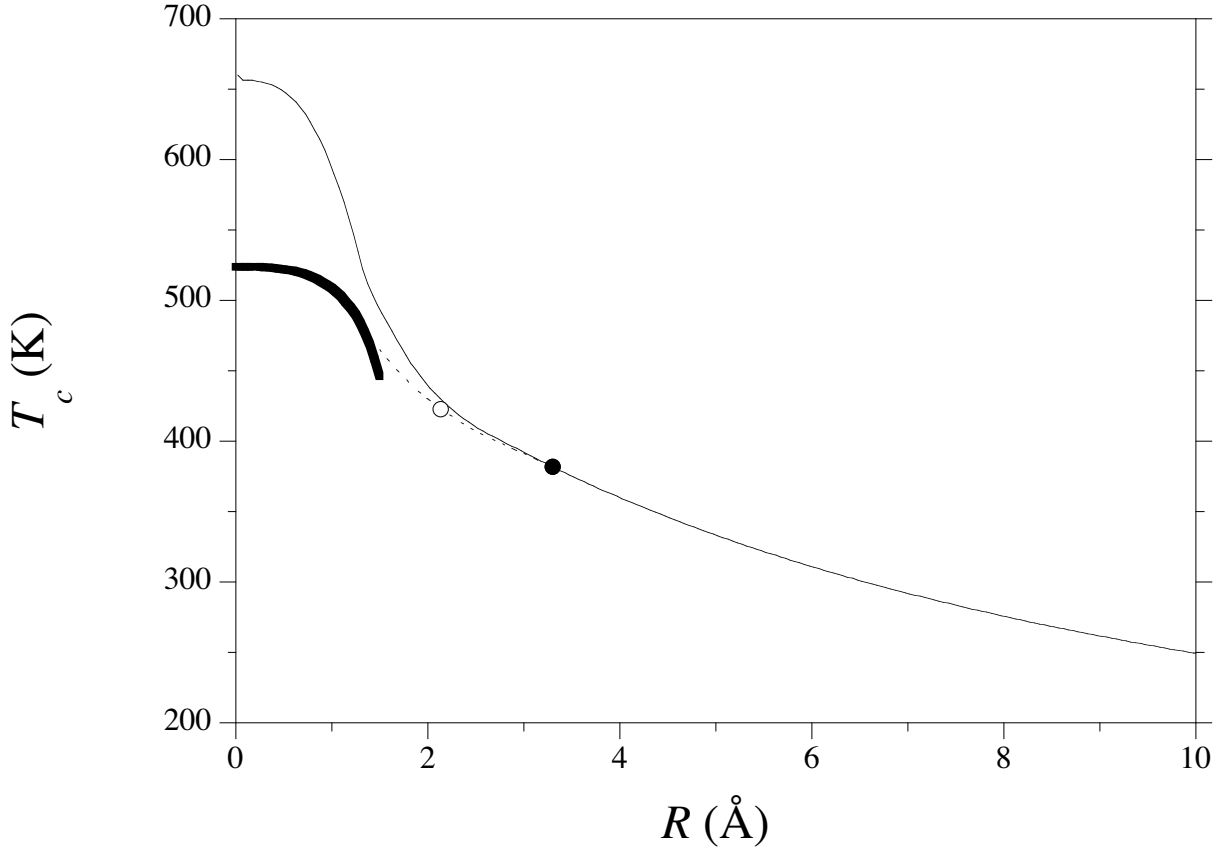


FIG. 13 Variation of the entropy convergence temperature with increasing HS radius. The thin solid line is the convergence temperature determined under the assumption the heat capacity is independent of temperature. The thick solid line is the exact entropy convergence temperature for spheres smaller than $R < \sigma_{WW}/2$, which satisfy Eq. 20. The dashed line smoothly interpolates between the exact and constant heat capacity curves at 1.25\AA and 3.3\AA , respectively. The filled circle indicates the entropy convergence temperature of a methane-sized solute ($T_c = 382\text{K}$). The open circle indicates the entropy convergence temperature based on the IT criterion ($T_c = 420\text{K}$).